Calculations for Piezoelectric Ultrasonic Transducers

Jensen, Henrik

Publication date:
1986

Document Version
Publisher's PDF, also known as Version of record

Risø-R-536

RISØ

Risø-R-536

Calculations for Piezoelectric Ultrasonic Transducers

Henrik Jensen

Risø National Laboratory, DK-4000 Roskilde, Denmark
May 1986

RISØ-R-536

CALCULATIONS FOR PIEZOELECTRIC ULTRASONIC TRANSDUCERS

Henrik Jensen

Abstract. Analysis of piezoelectric ultrasonic transducers implies a solution of a boundary value problem, for a body which consists of different materials, including a piezoelectric part. The problem is dynamic at frequencies, where a typical wavelength is somewhat less than the size of the body. Radiation losses as well as internal losses may be important. Due to the complexity of the problem, a closed form solution is the exception rather than the rule. For this reason, it is necessary to use approximate methods for the analysis.

(Continued next page)

May 1986
Risø National laboratory, DK 4000 Roskilde, Denmark

Equivalent circuits, the Rayleigh-Ritz method, Mindlin plate theory and in particular the finite element method are considered. The finite element method is utilized for analysis of axisymmetric transducers. An explicit, fully piezoelectric, triangular ring element, with linear variations in displacememnt and electric potential is given. The influence of a fluid half-space is also given, in the form of a complex stiffness matrix.

A special stacking procedure, for analysis of the backing has been developed. This procedure gives a saving, which is similar to that of the fast fourier transform algorithm, and is also wellsuited for analysis of finite and infinite waveguides.

Results optained by the finite element method are shown and compared with measurements and exact solutions. Good agreement is obtained.

It is concluded that the finite element method can be a valueable tool in analysis and design of ultrasonic transducers.

Thesis submitted in partial fulfilment of the requirements for the Lic.Techn. degree at the Technical University of Denmark.

ISBN 87-550-1198-5
ISSN 0106-2840

Grafisk Service 1986

CONTENTS

Page

PREFACE

The present work has been carried out at the structural Mechanics Section of Risø National Laboratory under the Lic. Techn. (Ph.D.) programme of the Technical University of Denmark.

The study was supervised by Professor, Lic. Techn. Leif Bjørnø, of the Technical University of Denmark, whose kind encouragement is greatly appreciated, and Dr. Tech. Steen Krenk at Risø National Laboratory. I wish especially to express my gratitude to Dr. Krenk for his valuable guidance and suggestions throughout the study.

The co-operation with the Medical R & D Group at Brüel & Kjær is greatly appreciated.

Hans E. Gundtoft and Torben Nielsen from the Metallurgy Department at Risø are thanked for providing access to the equipment for sound field characterization and for help with the measurements.

My other colleagues at the Structural Mechanics Sections, especially Ole Gunneskov, are thanked for inspiring conversations.

Finally, I would like to thank Ms. Kirsten Hansen who typed the manuscript and Ms. Agnete Michelsen who prepared the drawings.

Risø, 17 july, 1985
Henrik Jensen

1. INTRODUCTION

The use of ultrasound for such different purposes as industrial processing, non-destructive testing, and medical diagnostics has been known for more than thirty years [1,2]. The ultrasound can be generated and detected in a number of different ways. One of the methods that can be used both for generation and detection of ultrasound, is to utilize the piezoelectric effect. Piezoelectric transducers are the ones most commonly used, especially for ultrasonic imaging systems, where high frequencies are desirable [3]. In the following only piezoelectric transducers are considered.

The piezoelectric effect is the effect that some materials may produce an electric field, when they are subjected to stress or strain, and vice versa. The effect was first discovered in quarts by the brothers Pierre and Jacques Curie in 1880 [4].

Piezoelectric transducers may consist of several parts. The electro-mechanical energy conversion takes place in a piezoelectric plate. One or more matching layers may be placed on the front of it, to minimize the reflections from the interface between the transducer and the surrounding medium. A so-called backing may be attached to the back of the transducer, to damp the transducer, for obtaining a broader frequency range.

The various parts of the transducer possess different characteristics. The piezoelectric plate is inherently anisotropic. The backing is highly damping. The surrounding medium is normally considered to be an unbounded fluid. Probably due to these differences, and the complexity of the problem, the dominant method for analyzing complete transducer systems is equivalent circuits [5]; similar one-dimensional methods may also be used [6]. In the method of equivalent circuits, the parts of the transducer are represented by a lumped linear (electric) network. As the network topology and the parameters must be found by other methods, the equivalent circuit may be viewed as a convenient method to organize information obtained by other means.

Free vibrations of elastic [7,8], and piezoelectric [9,10] plates, at frequencies where the wavelength is comparable to the thickness of the plate, have been studied by many authors. They have generally obtained good results for the first few eigenfrequencies, but the methods are not easily applicable to analyses of transducers. Thus, the piezoelectric plate in a transducer often is assumed to vibrate in piston-like motion of a simple thickness stretch. As a first approximation the plate is estimated to be a half wavelength thick. A matching layer is then a quarter wave-length thick, and has a characteristic impedance, which is the geometric mean of the two neighbouring media. This result is well known from the theory of transmission lines [11, p 51], but only for one-dimensional problems. The backing and the surrounding medium can also be included in the analysis, but again via simplifying assumptions which leads to one-dimensional models.

The radiated field is naturally of great interest and much work has been done on radiation from various rigid pistons [12]. The impedance of a rigid circular piston was given by Rayleigh [13, §302], who found it by integrating the source distribution. The field on the axis is given by King [14]. He uses an integral transform technique. The effect of focusing has been considered by O'Neil [15]. Non-rigid pistons with polynomial velocity distributions have also been considered [16,17,18].

In contrast to the other methods, the finite element method can easily be used to analyze complete transducer systems. It can handle different materials, elastic as well as piezoelectric [19] in the same model. Internal damping as well as radiation losses may be included. As a consequence, the finite element method has become increasingly more used for analysis of piezoelectric transducers, during the last ten years [19-24]. This is probably also due to the decreasing cost of numerical computations.

The prime subject of this thesis is development and investigation of a method for analysis of piezoelectric transducers based on the finite element method. The transducer is in most cases assumed to be axisymmetric. The analysis assumes time harmonic exi-

tation, implicitly given by a timefactor $e^{-i\omega t}$. The equations of linear piezoelectricity are presented in Sec. 2 The three-dimensional equations are presented in tensor notation, whereas the axisymmetric equations are given in matrix notation. In Sec. 3 the most commonly used methods for analyzing transducer elements and complete transducers are outlined. The finite element method for axisymmetric structures, as used in the present project is the subject of Sec. 4. The load on the transducer is assumed to be a fluid half-space. Its influence on the vibrations of the transducer and the radiated soundfield are treated in Sec. 5. Section 6 is about a method for generating super elements, for cylindrical structures by a special stacking procedure. These super elements can be used to model waveguides, and are especially intended for modelling of the backing. The application of the method to infinite waveguides is also outlined. Two computer programs for finite element calculations on axisymmetric piezoelectric structures, are shortly described in Sec. 7 and example problems are given in Sec. 8.

2. THE EQUATIONS OF LINEAR PIEZOELECTRICITY

In accordance with the "IEEE Standard on Piezoelectricity" [25], and common practice in mechanical engineering, the following conventions, originally due to Einstein, are employed. Repeated indices imply summation over all allowable values of these indices. A comma followed by an index denotes a partial derivative with respect to a space coordinate. Time derivatives are denoted by a dot or the factor $-i\omega$, as only harmonic time dependence is considered. The indices i,j,k, and l may take the values 1 through 3. The indices α,β,γ the values 1 or 3, and finally the indices p and q the values 1 through 3 and 5.

2.1. General equations

Introduce a three-dimensional cartesian coordinate system (x_i) and let the displacements be given by

$$u_j = u_j(x_i) \tag{2.1}$$

The strain tensor S_{ij} is then derived as

$$S_{ij} = 1/2(u_{i,j} + u_{j,i}) \tag{2.2}$$

The electric potential ϕ is given by

$$\phi = \phi(x_i) \tag{2.3}$$

from which the electric field vector E_j is derived as

$$E_j = E_j(x_i) = - \phi_{,j} \tag{2.4}$$

The constitutive equations, which relate the strain tensor and the electric field vector to the stress tensor, T_{ij} and the electric displacement D_i, are derived from thermodynamic potentials.

Let the temperature be denoted by θ and the specific entropy by σ. The first law of thermodynamics then gives the differential of the internal energy U as

$$dU = \theta d\sigma + E_i dD_i + T_{ij} dS_{ij} \tag{2.5}$$

where $\theta d\sigma$ is the change in heat, and the remaining terms express the change in work done on the system. Magnetic effects are ignored for the case of piezoelectric materials. Otherwise a term $(H_i dB_i)$ for the magnetic work should have been included [26]. If the internal energy is considered as a function of σ, D_i, and S_{ij} only, its differential may be identified with (2.5) to give

$$\theta = \left(\frac{\partial U}{\partial \sigma}\right)_{D,S} \quad ; \quad E_i = \left(\frac{\partial U}{\partial Di}\right)_{\sigma,S} \quad ; \quad T_{ij} = \left(\frac{\partial U}{\partial Sij}\right)_{\sigma,D} \tag{2.6}$$

with the differentials

$$
\begin{aligned}
d\theta &= \left(\frac{\partial^2 U}{\partial \sigma^2}\right)_{D,S} d\sigma + \left(\frac{\partial^2 U}{\partial \sigma \partial D_k}\right)_S dD_k + \left(\frac{\partial^2 U}{\partial \sigma \partial S_{kl}}\right)_D dS_{kl} \\
dE_i &= \left(\frac{\partial^2 U}{\partial D_i \partial \sigma}\right)_S d\sigma + \left(\frac{\partial^2 U}{\partial D_i \partial D_k}\right)_{\sigma,S} dD_k + \left(\frac{\partial^2 U}{\partial D_i \partial S_{kl}}\right)_\sigma dS_{kl} \\
dT_{ij} &= \left(\frac{\partial^2 U}{\partial S_{ij} \partial \sigma}\right)_D d\sigma + \left(\frac{\partial^2 U}{\partial S_{ij} \partial D_k}\right)_\sigma dD_k + \left(\frac{\partial^2 U}{\partial S_{ij} \partial S_{kl}}\right)_{\sigma,D} dS_{kl}
\end{aligned}
\tag{2.7}
$$

When these equations are linearized, they give one set of constitutive equations, where the second-order partial derivatives of U are material constants. In most applications of piezoelectric materials the difference between isothermal and adiabatic processes is negligible, and the terms involving θ or σ may be ignored. The linearized form of (2.7) is then

$$
\begin{aligned}
T_{ij} &= c^D_{ijkl} S_{kl} - h_{kij} D_k \\
E_i &= - h_{ikl} S_{kl} + \beta^S_{ik} D_k
\end{aligned}
\tag{2.8}
$$

where superscripts D and S denote "at constant electric displacement" and "at constant strain".

Other constitutive equations may be derived from other thermodynamic potentials. S_{ij} and E_i have been derived from their potentials and are thereby assured to fulfil the equations of compatibility. It is desirable to have the constitutive equations with S_{ij} and E_i as independent variables. To substitute E_i for D_i as independent variable, a new thermodynamic potential is defined by adding $-E_i D_i$ to the internal energy.

$$H = U - E_i D_i \tag{2.9}$$

This potential is called the electric enthalpy [10, p. 34] and its differential is

$$dH = \theta d\sigma - D_i dE_i + T_{ij} dS_{ij} \tag{2.10}$$

The enthalpy is considered a function of σ, E_i and S_{ij} only, and the differentials of the complementary quantities become

$$\begin{aligned}
d\theta &= \left(\frac{\partial^2 H}{\partial \sigma^2}\right)_{E,S} d\sigma + \left(\frac{\partial^2 H}{\partial \sigma \partial E_k}\right)_{S} dE_k + \left(\frac{\partial^2 H}{\partial \sigma \partial S_{kl}}\right)_{E} dS_{kl} \\
dD_i &= -\left(\frac{\partial^2 H}{\partial E_i \partial \sigma}\right)_{S} d\sigma - \left(\frac{\partial^2 H}{\partial E_i \partial E_k}\right)_{\sigma,S} dE_k - \left(\frac{\partial^2 H}{\partial E_i \partial S_{kl}}\right)_{\sigma} dS_{kl} \\
dT_{ij} &= \left(\frac{\partial^2 H}{\partial S_{ij} \partial \sigma_k}\right)_{E} d\sigma + \left(\frac{\partial^2 H}{\partial S_{ij} \partial E_k}\right)_{\sigma} dE_k + \left(\frac{\partial^2 H}{\partial S_i \partial S_k}\right)_{\sigma,E} dS_{kl}
\end{aligned} \tag{2.11}$$

If again these equations are linearized and thermal terms are ignored, the constitutive equations become

$$\begin{aligned}
T_{ij} &= C^E_{ijkl} S_{kl} - e_{kij} E_k \\
D_i &= e_{ikl} S_{kl} + \varepsilon^S_{ik} E_k
\end{aligned} \tag{2.12}$$

Here again the superscripts denote quantities to be kept constant. As these are the constitutive equations to be used throughout, the superscripts will not be written explicitly from now on. This equation is equivalent with (2.8), and could be derived from it, but can now be used to find the relations between the various material constants.

The material dependent tensors C_{ijkl}, e_{ikl} and ε_{ik} fulfil the following set of symmetry conditions

$$C_{ijkl} = C_{jikl} = C_{ijlk} = C_{klij}$$

$$e_{ikl} = e_{ilk} \tag{2.13}$$

$$\varepsilon_{ik} = \varepsilon_{ki}$$

This is partly due to the symmetry of S_{ij} and T_{ij} and partly due to the fact, that the electric enthalpy is an exact differential.

The Lagrangian, which conforms to the choice of S_{ij} and E_i as independent variables in the constitutive equations, must include the enthalpy in place of the potential energy [10, p. 44] and hence is given by

$$L = \int_V (1/2\rho \dot{u}_i \dot{u}_i - H(S_{ij}, E_k))dV \tag{2.14}$$

The virtual work done by external forces and the electric charge is

$$\delta W = \int_V (f_i^V \delta u_i - q^V \delta\phi)dV + \int_S (f_i^S \delta u_i - q^S \delta\phi)dS \tag{2.15}$$

where V is the volume of the considered system, and S is its surface.

f_i^V and f_i^S are forces applied to the volume or the surface of the body as q^V and q^S, respectively, are externally induced electric charge in V and on S.

The equations of motion, Gauss' law for the electric displacement and the boundary conditions are now contained in Hamilton's principle

$$\delta \int_{t_o}^{t_i} L dt + \int_{t_o}^{t_i} \delta W dt = 0 \tag{2.16}$$

As may be seen by writing (2.16) as

$$\int_{t_o}^{t_i} \{ \int_V (T_{ij,j} + f_i^V - \delta\ddot{u}_i)\delta u_i dV + \int_V (D_{i,i} - q^V)\delta\phi dV \tag{2.17}$$

$$- \int_S (T_{ij}n_j - f_i^S)\delta u_i dS - \int_S (D_i n_i + q^S)\delta\phi dS \} dt = 0$$

(2.17) must hold for arbitrary variations δu_i, $\delta\phi$ inside V, and so it is concluded that

$$T_{ij,j} + f_i^V = \rho\ddot{u}_i \tag{2.18}$$

and

$$D_{i,i} = q^V \tag{2.19}$$

The first is the equation of motion, and the second is one of the Maxwell equations, which is known as Gauss' law for the electric displacement.

On the part of the surface where δu_i is arbitrary, it can further be concluded that

$$T_{ij}n_j = f_i^S \tag{2.20}$$

whereas the displacements must be prescribed on the remaining part. Likewise, it can be concluded that

$$D_i n_i = -q^S \tag{2.21}$$

on the part of the surface, where $\delta\phi$ is arbitrary. ϕ is prescribed on the remaining part. These results are derived along the lines of H.F. Tiersten [10]. He also points out that (2.17) is not as useful for obtaining approximate solutions for prescribed displacements and electric potentials as for prescribed stress and electric charge. The reason for this is that the variations of u_i and ϕ are constrained to vanish on those parts of the boundary on which they are prescribed and any approximating function used in the principle must satisfy this constraint

too. Tiersten also performs the necessary modifications to overcome this and to include discontinuity surfaces [10, Ch. 6.4].

2.2. Axisymmetric equations

If the physical problem at hand is such that there is no dependence of the angular variable θ in a properly chosen cylindrical coordinate system, the problem is said to be axisymmetric. The equations can be reduced to two dimensions, and great savings can be obtained this way. This can happen only if the materials are isotropic or transversely isotropic with the normal to the planes of isotropy orientated in the direction of the axis of symmetry. Crystals of crystallographic class 6mm and poled ferroelectric ceramics - the so-called piezoelectric ceramics - are important examples of such materials. The two-dimensional axisymmetric equations can be derived from the three-dimensional equations in cylindrical coordinates, formally by setting tangential components u_θ, E_θ, etc. to zero as well as all derivatives with respect to the angular variable $\partial/\partial\theta = 0$. The displacement-strain relations can be found in any standard textbook on elasticity theory [27, p. 5]. The electric field vector is minus the gradient of the electric potential. With an appropriate indexing of the strains and the electric field, the constitutive equations are still given by (2.12). The equations of motion can be found in [27, p. 90]. When the condition of axial symmetry is enforced on the general equations in cylindrical coordinates the following two-dimensional equations are obtained. They will be presented in compressed matrix notation with omission of components that are always zero.

Introduce a two-dimensional cartesian coordinate system (x_1, x_3) where x_1 is the radial coordinate and x_3 is the axial coordinate. Let the displacement vector be

$$S_p = \begin{Bmatrix} S_1 \\ S_2 \\ S_3 \\ S_5 \end{Bmatrix} = \begin{Bmatrix} u_{1,1} \\ u_1/x_1 \\ u_{3,3} \\ u_{1,3} + u_{3,1} \end{Bmatrix} \tag{2.23}$$

the indices p (and q) may take the values 1,2,3 and 5. The electric field vector is

$$E_\alpha = - \phi_{,\alpha} \tag{2.24}$$

where ϕ is the electric potential. The constitutive equations are

$$\begin{aligned} T_p &= C_{pq}\, S_q - e_{\beta p}\, E_\beta \\ D_\alpha &= e_{\alpha q}\, S_q + \varepsilon_{\alpha\beta}\, E_\beta \end{aligned} \tag{2.25}$$

where

$$C_{pq} = \begin{Bmatrix} C_{11} & C_{12} & C_{13} & 0 \\ C_{12} & C_{11} & C_{13} & 0 \\ C_{13} & C_{13} & C_{33} & 0 \\ 0 & 0 & 0 & C_{55} \end{Bmatrix} = \begin{Bmatrix} C_{1111} & C_{1122} & C_{1133} & 0 \\ C_{1122} & C_{1111} & C_{1133} & 0 \\ C_{1133} & C_{1133} & C_{3333} & 0 \\ 0 & 0 & 0 & C_{1313} \end{Bmatrix} \tag{2.26a}$$

$$e_{\alpha q} = \begin{Bmatrix} 0 & 0 & 0 & e_{15} \\ e_{31} & e_{31} & e_{33} & 0 \end{Bmatrix} = \begin{Bmatrix} 0 & 0 & 0 & e_{113} \\ e_{331} & e_{331} & e_{333} & 0 \end{Bmatrix} \tag{2.26b}$$

$$\varepsilon_{\alpha\beta} = \begin{Bmatrix} \varepsilon_{11} & 0 \\ 0 & \varepsilon_{33} \end{Bmatrix} \tag{2.26c}$$

For completeness it is noteworthy that the remaining non-zero material constants are related to those given in (2.26) by

$$C_{44} = C_{2323} = C_{55} = C_{1312}$$

$$C_{66} = C_{1212} = \frac{1}{2}(C_{11} - C_{12}) = \frac{1}{2}(C_{1111} - C_{1122}) \tag{2.27}$$

$$e_{24} = e_{223} = e_{15} = e_{113}$$

$$\varepsilon_{22} = \varepsilon_{11}$$

The equations of motion are given by

$$T_{1,1} + \frac{1}{x_1}(T_1 - T_2) + T_{5,3} + f_1^v = \rho\ddot{u}_1 \tag{2.28}$$

$$T_{3,3} + \frac{1}{x_1} T_5 + T_{5,1} + f_3^v = \rho\ddot{u}_3$$

and Gauss' law for the electric displacement is given by

$$D_{1,1} + \frac{1}{x_1} D_1 + D_{3,3} = q^v \tag{2.29}$$

3. METHODS FOR ANALYSIS OF PIEZOELECTRIC VIBRATIONS

The complexity of the piezoelectric boundary value problem precludes closed-form solutions in all but the simplest cases. In many applications of piezoelectric materials, solutions based on simplifying assumptions will, however, be fully acceptable. To the extent where simplifications are unacceptable, approximate solutions may be obtained by use of variational methods. The com-

promise between simplifying assumptions, and approximate solutions, has led to a number of different methods for solving the piezoelectric boundary value problem for various applications.

3.1. Direct solution

If the piezoelectric body is of simple shape, and if some dimensions are so different from the others that they need not to be considered finite, the problem may become simple enough for direct solution. This can be facilitated further, if the body can be considered isotropic elastic. Even in that case closed-form solutions seem to be obtainable only in few cases, which is probably due to the impossibility of representing the problem via a simple scalar potential as in acoustics.

Free vibrations of infinite elastic plates have been studied in detail by Mindlin [7, Ch. 2] and vibrations of piezoelectric plates have also been studied [10]. The problem of simple thickness vibrations of an infinite piezoelectric ceramic plate will be solved to serve as an example and because the solution of this problem plays an important role in transducer design. A similar solution for a plate of Y-cut quartz is given by Tiersten [10, p. 87-93]. Y-cut means that the plate is cut with its faces parallel to one of the hexagonal faces of a quartz crystal.

Let the plate be bounded by the planes $x_3 = \pm h$ in a cartesian coordinate system.

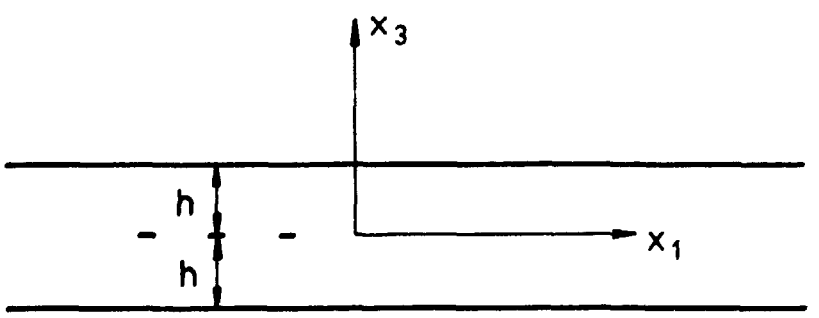

Fig. 3.1. Infinite plate of thickness 2h.

These planes are termed the faces of the plate. The vibrations of the plate are supposed to be simple in the sense that there is no dependence of the lateral coordinates x_1 and x_2. The only non-zero strains are then S_{i3} and S_{3i}. The only non-zero component of the electric field is E_3. These are substituted into the constitutive equations (2.12) to get the stress tensor and the electric displacement. The stresses and the electric displacement are again substituted into the equation of motion (2.19) and Gauss equation for the electric field (2.19), whereby the following system of differential equations is obtained

$$\frac{1}{2} C_{1313}\, u_{n,33} = \rho \ddot{u}_n; \quad n = 1,2$$

$$\begin{aligned} e_{333}\, \phi_{,33} + \quad & C_{3333}\, u_{3,33} = \rho \ddot{u}_3 \\ -\varepsilon_{33}\, \phi_{,33} + \quad & e_{333}\, u_{3,33} = 0 \end{aligned} \tag{3.1}$$

If only time harmonic variations are considered, the equations are reduced to a set of ordinary differential equations. The system of equations consists of two parts, one of which is the uncoupled equations for u_1 and u_2. The eigensolutions to this part are called the thickness shear modes. Their solutions are trigonometric functions of x_3. The arbitrary constants are determined by the boundary conditions of the shear stress. These vibrations cannot be excited electrically.

The other set of solutions are the coupled solutions for u_3 and ϕ. The electric potential may be eliminated to give

$$\left(\frac{e_{333}^2}{\varepsilon_{33}} + C_{3333}\right) u_{3,33} = C_{3333}^{*}\, u_{3,33} = \rho \ddot{u}_3 \tag{3.2}$$

where C_{3333}^{*} is the piezoelectrically stiffened elastic constant. The time harmonic solution is again trigonometric.

$$u_3 = A \cos(kx_3) + B \sin(kx_3) \tag{3.3}$$

where

$$k = \omega \frac{\rho}{\sqrt{C^*_{3333}}} \tag{3.4}$$

These vibrations can be electrically driven via the boundary conditions which are

$$\begin{aligned} \phi(h) - \phi(-h) &= 2\phi_- \\ T_{33}(h) \pm T_{33}(-h) &= 2\tau_\pm \end{aligned} \tag{3.5}$$

The arbitrary constants, A and B are determined by demanding the solution (3.3) to fulfil the boundary conditions, to be

$$\begin{aligned} A &= \frac{h\tau_-}{C^*_{3333} kh \sin(kh)} \\ B &= \frac{h\tau_+ - e_{333}\phi_-}{C^*_{3333} kh \cos(kh) - (C^*_{3333} - C_{3333})\sin(kh)} \end{aligned} \tag{3.6}$$

This shows that an infinite piezoelectric plate has two sets of simple thickness stretch modes. Modes, for which the series of eigenfrequencies is harmonic, and the displacements and the electric potential are symmetric around the midplane. Therefore, they cannot be excited electrically. The other set consists of antisymmetric modes with eigenfrequencies that are not integral multiple of a fundamental eigenfrequency, but may be determined from the equation

$$\left(1 + \frac{\varepsilon_{33} C_{3333}}{e^2_{333}}\right) kh = \tan(kh) \tag{3.7}$$

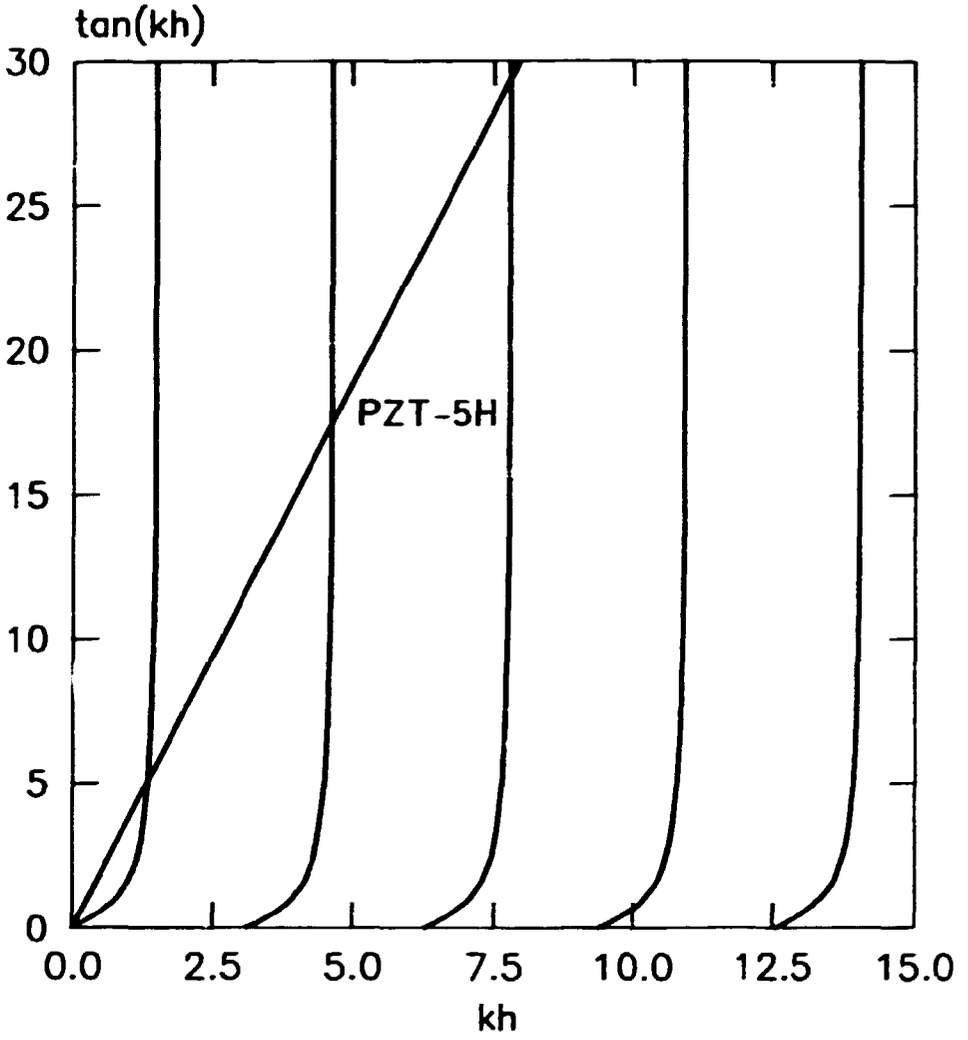

Fig. 3.2. tan(kh) and $kh \cdot (1 + \varepsilon_{33} C_{3333} / e_{333}^2)$. The intercepting points give the values of kh for the simple thickness stretch modes in an infinite plate.

In any event, the lowest of the eigenfrequencies (>0) is called the fundamental thickness eigenfrequency. The product of this frequency and the thickness of the plate is specific for a certain material. It is often included in the material data, under the name of the thickness eigenfrequency constant or N_t . i.e. $N_t = k_1 hc/\pi$.

In many cases is neither the stresses nor the velocities known on the faces of a plate. But their ratios, commonly known as the

acoustic impedances, Z, may be known approximately. This may be the case, if the plate is in contact with a fluid on its two faces. The acoustic impetance is then ρcA, where A is the area of the plate. ρc, the product of the mass density and the sound velocity in the fluid, is called the specific acoustic impedance of the fluid.

If the half sum and difference of the acoustic impetances on the two sides of the plate is denoted by Z_+ and Z_- respectively, the stresses can be found from

$$Z_+ = i(\tau_- + \tau_+)/\omega u_3(h)$$
$$Z_- = i(\tau_- - \tau_+)/\omega u_3(-h) \tag{3.8}$$

in which case A and B become

$$A = \frac{i\omega h(Z_+ - Z_-)\sin\xi}{D} e_{333}\phi_- \tag{3.9}$$

$$B = \frac{-i\omega h(Z_+ + Z_-)\cos\xi - 2C^*\xi\sin\xi}{D} e_{333}\phi_-$$

with

$$D = -C^*\xi C' + C^*\xi(C' + i\omega h(Z_+ + Z_-))\cos 2\xi$$
$$+ ((C^*\xi)^2 + (\omega h)^2 Z_+ Z_- - \tfrac{1}{2} i\omega C' h(Z_+ + Z_-))\sin 2\xi \tag{3.10}$$

where $\xi = kh$, $C^* = C^*_{3333}$, and $C' = C^*_{3333} - C_{3333}$.

The solution for the simple thickness-stretch vibration is useful for one-dimensional analyses of transducers because of their simplicity, and because these vibrations produce waves in a fluid. For these solutions to be valid, the thickness of the plate must be small in comparison with any lateral dimension. If the plate

is thin and vibrating freely, solutions may also be found by assuming the plate to be in a state of planar stress. For circular plates a set of so-called radial modes can be found this way [28]. The frequency equation for the radial modes may be given in a form, much like the frequency equation for the simple thickness vibrations (3.7)

$$\frac{1}{1-\nu_p}\, ka = \frac{J_1(ka)}{J_0(ka)} \tag{3.11}$$

where J_1 ( ) and J_0( ) are Bessel functions, k is the wave number, a the radius, and ν_p the planar Poisson's ratio defined by

$$\nu_p = \frac{c_{1122}c_{3333} - c_{1133}^2}{c_{1111}c_{3333} - c_{1133}^2}$$

It may be noticed that the piezoelectric properties do not influence the eigenfrequencies of the radial modes, and that the coefficient to ka in (3.11) for isotropic media is always between unity and two.

The values of ka which satisfy the frequency equation may be found as the intercepting points between the function $J_1(ka)/J_0(ka)$, which is shown on Fig. 3.3, and the straight line through the origin with a slope of $(1-\nu_p)^{-1}$.

It can be seen that the eigenfrequencies of the higher radial modes are very insensitive to the value of ν_p, and that ka asymptotically becomes equal to the zeros of J_1.

The existence of radial modes also shows that the presence of edges is important, even in thin plates.

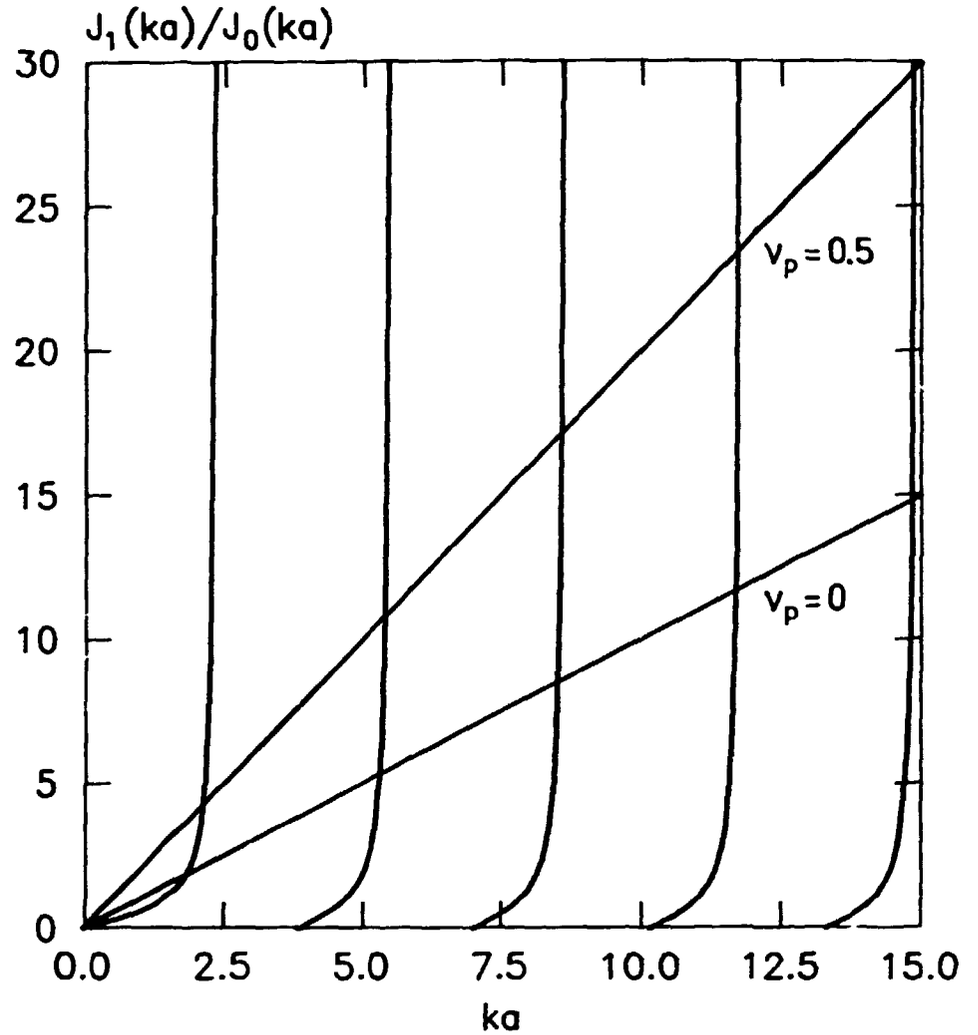

Fig. 3.3. $J_1(ka)/J_0(ka)$ and $ka/(1-\nu_p)$ for $\nu_p = 0$ and 0.5. The intercepting points give the values of ka for the radial modes in circular plate. (c.f. Fig. 3.2)

3.2. Equivalent circuits

A commonly used method for analysis of piezoelectric transducers especially by electrical engineers is the equivalent circuit. The equivalent circuit for an electro-mechanical system is a linear electric network, which, when substituted for the system in any electric circuit, has the same effect as the system itself, at least in a limited frequency range.

If the mechanical system is lumped, the equivalent circuit may be obtained directly by an analogy [5]. The analogies are based on the fact that both systems are governed by linear second order, ordinary differential equations.

The system in Fig. 3.4 is governed by the equation

$$F = K \int v \, dt + M \dot{v} \tag{3.12}$$

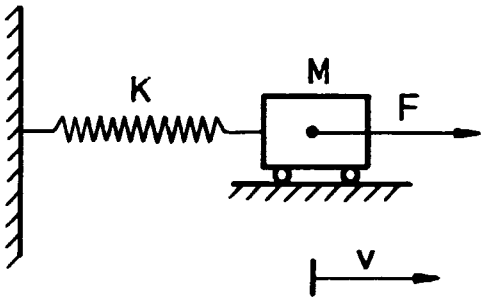

Fig. 3.4. Spring/mass system with one degree of freedom.

where v is the velocity of the node. The most commonly used analogy is the so-called impedance analogy [29]. Here the force is considered equivalent to an electric voltage (electromotive force) and the velocity to an electric current. An electric network, which consists of a capacitor with the capacitance K^{-1}, and a coil with an inductance of M in serial connection, would be governed by the same equation.

Another analogy, which is known as the admittance, or inverse, analogy is obtained simply by taking the dual electric network. For a network with more degrees of freedom, several analogies may be obtained by combining the two. Only the impedance analogy will be treated in the following.

Although the spring and the mass in Fig. 3.4 at first may look as if they were connected in series they are connected in parallel from a network theoretical point of view. This is because the lumped mass M must be viewed as a two-terminal element where the other terminal is connected to the inertial system (ground). As

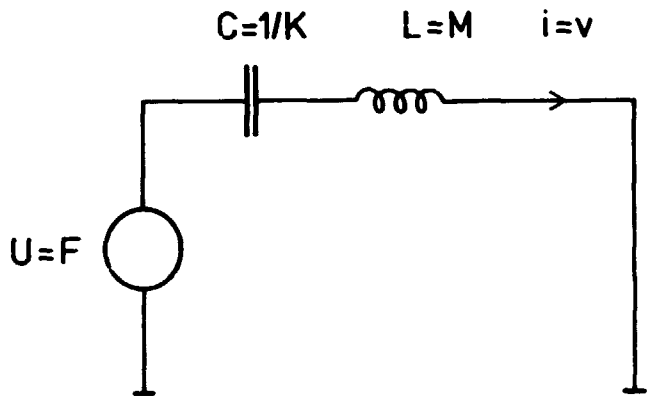

Fig. 3.5. Electric equivalent to the mechanical system in Fig. 3.4.

the spring also has one terminal connected to ground they are coupled in parallel. The impedance analogy for mechanical systems gives electric networks which are topological inverse to the mechanical systems (dual). The impedance analogy is summarized in Table 3.1.

Table 3.1. Equivalent mechanical and electrical quantities in the impedance analogy.

Mechanical	Electrical
Force	Voltage
Velocity	Current
Compliance	Capacitance
Mass	Inductance
Damping (viscos)	Resistance

In continuous systems, the equivalent circuit can be based on the existence of an infinite number of (complex) eigenfunctions and corresponding (complex) eigenfrequencies. Each of these can be treated as if it had only a single degree of freedom. Consequently, each mode may be represented by the equivalent circuit shown in Fig. 3.6

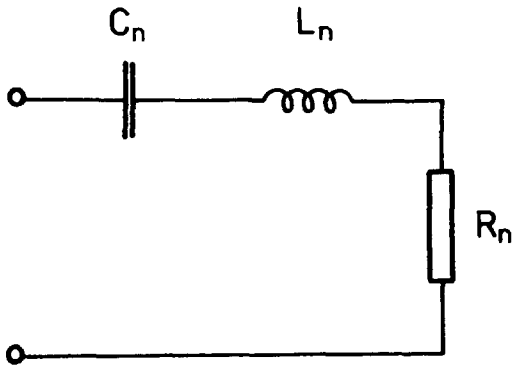

Fig. 3.6. Equivalent circuit for a single mode, in a continuous system.

The equivalent circuit will then have the same eigenfrequency and damping as the mode it models, but there is an undetermined scaling factor, which depends on what quantities the voltage and the current in the circuit represent. A complete equivalent curcuit can be constructed by connecting all pertinent single mode equivalent circuits in parallel. The method is attractive only when the number of encounted modes is low. Often, the equivalent circuit will include only one mode.

In electro-mechanical systems the coupling may be modelled by an (ideal) transformer. The equivalent circuit for an ultrasonic transducer could be the one shown on Fig. 3.7. The voltage on the primary side of the transducer is the voltage across the electrodes, $2\Phi_-$ and the current on the secondary side, v, represents the average velocity of the face of the transducer.

The capacitor C_o represents the purely electric capacitance of the clamped transducer. The other network parameters could be found by measurements and/or from solutions based on greatly sim-

plifying assumptions. If the tansducer consists only of a thin plate, the boundary conditions on the edges of the plate are often assumed to be unimportant, and the solution for simple thickness vibrations may be employed.

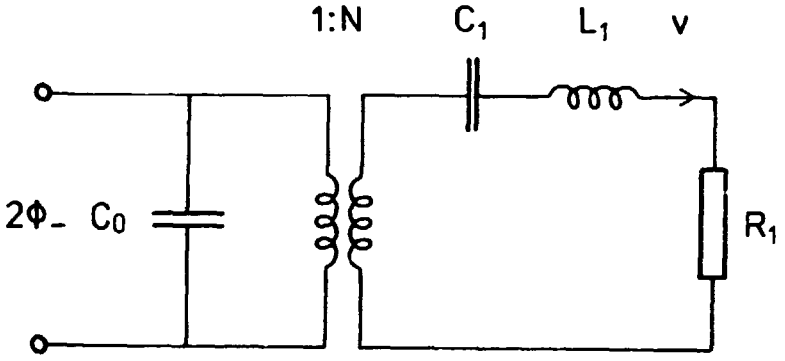

Fig. 3.7. Equivalent circuit for an ultrasonic transducer near a single eigenfrequency.

The velocity of the faces of the unloaded lossless infinite plate is found from (3.3) and (3.6) to be

$$v = \frac{-i\omega e_{333}\Phi_-}{C^*_{3333}(kh\ \cot(kh) - 1) + C_{3333}} \tag{3.13}$$

From the equivalent circuit it is found to be (with $R_1 = 0$)

$$v = \frac{-i\omega N\Phi_-}{-L_1\omega^2 + \frac{1}{C_1}} \tag{3.14}$$

where $N = e_{333}A/h$, and A is the area of the plate. L_1 and C_1 are then chosen so that (3.14) gives the best match to (3.13) in the frequency range of interest. The low-frequency match is obtained by $L_1 = 1/3\ \rho hA$ and $C_1 = h/(AC_{3333})$. The match near the technically more important fundamental thickness mode is obtained by matching the Taylor expansions of the denominators around the first zero of the denominator in (3.13). This leads to

$$\frac{1}{\sqrt{L_1 C_1}} = \omega_1$$

$$\frac{L_1}{\sqrt{C_1}} = \frac{-A}{2h} d'(\omega_1) \qquad (3.15)$$

where ω_1 is found by solving (3.7), and $d(\omega)$ is the denominator of (3.13). The denominator may be approximated by $C^*_{3333}khcot(kh)$ and the solution given by Mason [5, p. 206] is obtained, for which $kh = \pi/2$. The component values then become $L_1 = 1/2\rho hA$ and $C_1 = 8/\pi^2 \cdot h/(AC^*_{3333})$. The frequency response for the facial displacements of an infinite plate is compared to that given by

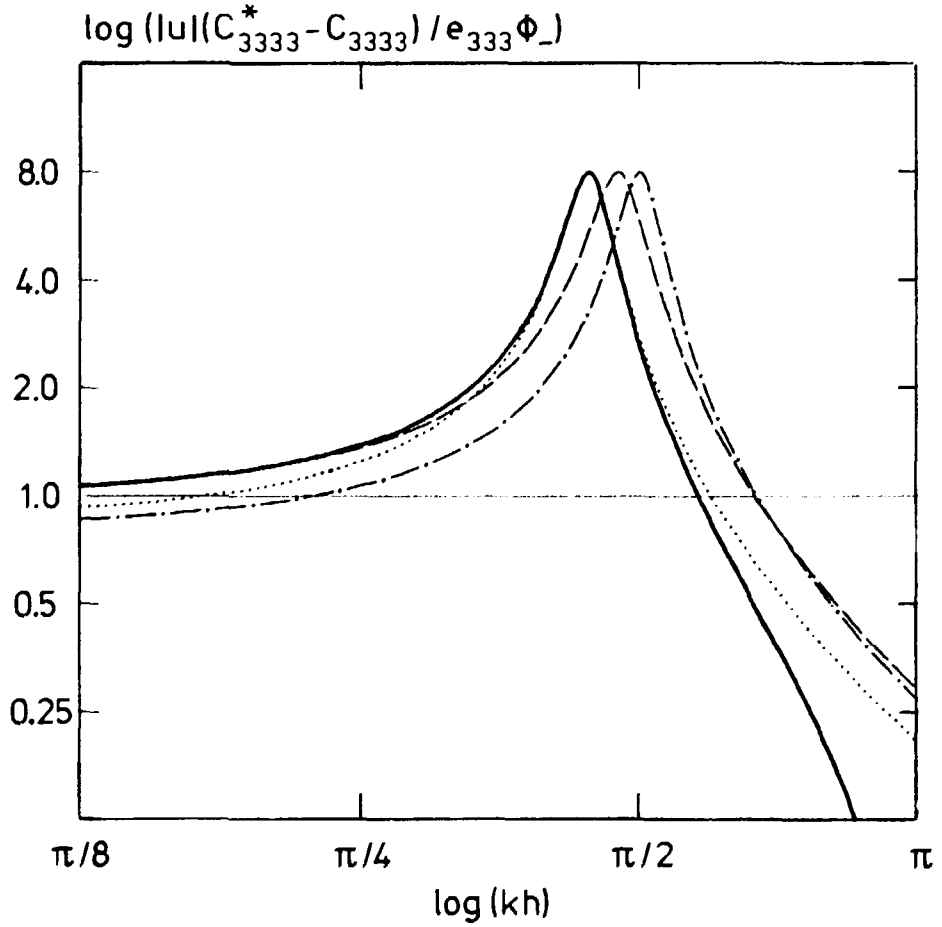

Fig. 3.8. Frequency response for the displacement of an infinite plate (-) compared with those given by matched equivalent circuits. $(C^*_{3333}-C_{3333})/C_{3333} = 0.3804$.

use of equivalent circuits in Fig. 3.8. The solid line shows the ressponse from the infinite plate. The dashed-dotted line show Mason's solution. The low-frequency match is shown by the dashed line, and the match near the thickness eigenfrequency is shown by the dotted line.

If the plate is submerged into a fluid, it will be damped. As a first approximation this may be included in the equivalent circuit by assigning a value of $\rho_{f1}c_{f1}$ A to R_1. $\rho_{f1}c_{f1}$ is the specific acoustic impedance of the fluid. In general, the radiation impedance for finite plates is both complex and frequency dependent.

The radiation impedance is treated in more detail in Section 5. If the radiation impedance is not small compared with the impedance due to the stiffness of the piezoelectric plate, the velocity in (3.13) must be found on the basis of the equation for a loaded plate (3.9) instead of simpler equation for a free plate (3.6).

3.3. Mindlin plate theory

The free vibrations of circular piezoelectric disks have been analysed with second-order Mindlin plate theory by several authors [30,31,32] and good agreement with measurements [33,32] has been obtained, at least for the eigenfrequencies.

A plate is characterized by being smaller in the thickness direction, here x_3, than in the other directions. The variations in the thickness direction can be expanded in a power series [7] or in orthogonal polynomials [34], in which case the expressions become a little simpler. If the faces of the plate are given by $x_3 = \pm h$, the polynomial expansion becomes

$$u_j(x_i) = \sum_{n=0}^{\infty} P_n(x_3/h)\, u_j^{(n)}(x_1,x_2) \qquad (3.16)$$

where $P_n(\ )$ is the Legendre polynomial of degree n.

When the expansions for u_j are substituted into a three-dimensional variational principle as e.g. Hamilton's principle (2.16), and the integration across the thickness is performed, the three-dimensional equations are converted into an infinite set of two-dimensional equations. These equations are truncated to a finite set of equations. The exact solution for an infinite plate is used to decide additional terms to be discarded and to determine a set of correction coefficients [34]. During the process of truncation stress components are also discarded and both the constitutive equations and the equations of motion are satisfied only in an average sense. Plate theory where only expansion coefficients up to n = 2 are retained is called second-order theory. Second order theory works satisfactorily for frequencies up to well above the thickness eigenfrequency. The present author is unaware of uses of Mindlin plate theory of higher order. The theory has also been extended to cover the piezoelectric case [10, Chapter 13], but free vibrations are primarily determined by the mechanical characteristics. This is not the case for damped electrically driven vibrations.

3.4. The Rayleigh-Ritz method

The Rayleigh-Ritz method is well-known from the calculus of variations for obtaining approximations to a function, f, which makes some functional, G, stationary

$$\delta G = \delta \int_V F(x_i, f(x_i), f(x_i)_{,j}) dV \ . \tag{3.17}$$

This is done by choosing a test function, f, which is a function of N additional parameters, a_n. The approximating function is then obtained by solving the equations

$$\frac{\partial G}{\partial a_n} = 0, \quad ; \quad n = 1,2, \ldots, N \tag{3.18}$$

This method has been used for many years in the field of mechanics, but it was first applied to piezoelectric materials in 1967 by Holland and Eer Nisse [35,36], who found their functional G by a trial and error method. The functional may, however, also be derived from Hamilton's principle (2.16). The variations must vanish in the time limits, t_o, t_1 which in the case of no losses and harmonic excitation can be obtained for $t_o = -\pi/2\omega$ and $t_1 = \pi/2\omega$. The time factor $e^{-i\omega t}$ will then cause (the real part of) the variations in u_i and ϕ to vanish at t_o and t_1. The kinetic energy, on the other hand, is a function of u_i and the variations of $\dot{u}_i$ do not vanish. This is why the time derivatives must be "moved" by partial integration to give

$$\delta \int_{t_o}^{t_i} dt \int_V \rho \dot{u}_i \dot{u}_i dV = - \delta \int_{t_o}^{t_i} dt \int_V \rho \ddot{u}_i u_i dV \tag{3.19}$$

The time integration in Hamilton's principle can then be replaced by an unimportant factor $-2/\omega$, which is replaced by -1 to give the functional

$$G = \frac{1}{2} \int_V (-\omega^2 \rho u_i u_i + S_{ij} C_{ijk\ell} S_{k\ell} - 2E_k e_{kij} S_{ij} - E_i \varepsilon_{ij} E_j) dV$$
$$- \int_S (f_i^S u_i - q^S \phi) ds \tag{3.20}$$

where f_i^V and q^V in (2.15) are assumed to be zero, and the volume integral is then the Lagrangian (2.14).

The displacements and the electric potential are then substituted by

$$u_i = \sum_{m=1}^{M} a_m u_i^{(m)}$$
$$\phi = \sum_{m=1}^{M} a_m \phi^{(m)} \tag{3.21}$$

where $(u_i^{(m)}, \phi^{(m)})$ are test functions and the unknown coefficients a_m are determined from

$$\frac{\partial G}{\partial a_n} = \int_S (q^S \phi^{(n)} - f_i^S u_i^{(n)}) ds$$

$$+ \sum_{m=1}^{M} a_m \int_V \{ - \omega^2 \rho u_i^{(m)} u_i^{(n)} + u_{i,j}^{(m)} C_{ijkl} u_{k,l}^{(n)} \tag{3.22}$$

$$+ \phi_{,k}^{(m)} e_{kij} u_{i,j}^{(n)} + \phi_{,k}^{(n)} e_{kij} u_{i,j}^{(m)}$$

$$- \phi_{,i}^{(m)} \varepsilon_{ij} \phi_{,j}^{(n)} \} \, dV = 0$$

The admissible testfunction are those that fulfil the boundary conditions for u and ϕ, this is a consequence of the form of Hamilton's principle and, as pointed out last in Section 2.1, this restriction can be removed.

The choice of test functions greatly affects the problem of solving (3.22), and the obtainable accuracy of the solution. Eer Nisse applied this method to a freely vibrating thick disk [35] and compared the results with Shaw's experimental results [33]. The test functions were chosen as products of trigonometric functions in the thickness direction and Bessel functions in the radial direction. The different parameters were chosen so that the trigonometric functions were solutions for simple thickness vibrations of an elastic plate, and the Bessel functions were solutions for thin disks (see Section 3.1). With about thirty test functions Eer Nisse calculated the lowest (eight) eigenfrequencies to within 1% of the measured values. The number of test functions is quite high to obtain this result. Especially as first modes must be expected to closely resemble the radial modes. The priezoelectric coupling could be taken into account in the choice of test functions. The solution is not separable and coupling could be included too.

3.5. Finite element method

The finite element method is well established in structural mechanics [37,38]. It can be viewed as a special case of the Rayleight-Ritz method, where the whole body is divided into finite elements. The elements are defined via a number of nodes, where each element is given by the nodes it spans. The independent variables are normally the displacement components, and in piezoelectricity the electric potential as well. Within each element they are interpolated from their values in the nodal points of the element and a set of shape functions.

$$u_i(x_j) = \Sigma_n N_i^n(x_j) u_i^n \quad ; \quad \text{no sum over } i$$
$$\phi(x_j) = \Sigma_n N_4^n(x_j) \phi^n \tag{3.23}$$

where u_i^n and ϕ^n are the values of u and ϕ in node number n. N_i^n, N_4^n are the shape functions associated with node number n. They are normally zero in all other nodes and unity in the actual node

$$N_i^n(x_j^m) = \delta_{nm} \tag{3.24}$$

The shape functions are identically zero in all elements which do not share the actual node. In the sense of the Rayleigh-Ritz method, the shape functions play the role of test functions, and the nodal values play the role of parameters. With the shape functions inserted in the functional, G (3.20), the stationarity condition (3.22) can be written

$$\left(\begin{Bmatrix} K_{ij}^{nm} & K_{i4}^{nm} \\ K_{4i}^{nm} & K_{44}^{nm} \end{Bmatrix} - \omega^2 \begin{Bmatrix} M_{ij}^{nm} & 0 \\ 0 & 0 \end{Bmatrix} \right) \begin{Bmatrix} u_i^n \\ \phi^n \end{Bmatrix} = \begin{Bmatrix} F_j^m \\ -Q^m \end{Bmatrix} \tag{3.25}$$

where

$$(K_{ij}^{nm} - \omega^2 M_{ij}^{nm}) = \frac{\partial^2 L}{\partial u_i^n \partial u_j^m}$$

$$K_{i4}^{nm} = \frac{\partial^2 L}{\partial u_i^n \partial \phi^m} \qquad (3.26)$$

$$K_{44}^{nm} = \frac{\partial^2 L}{\partial \phi^n \partial \phi^m}$$

L is the Lagrangian. The K matrices together are called the generalized stiffness matrix and receive contributions only from the potential energy. M_{ij}^{nm} is called the mass matrix and receives contributions from the kinetic energy term of the Lagrangian. F_j^m is a vector of equivalent nodal forces and is also found from the stationarity condition of G. It receives contributions only from the work done by external forces, W.

$$F_j^m = -\frac{\partial W}{\partial u_j^m} = \int_s f_j^s N_k(x_i) ds; \quad \text{for } k = j \qquad (3.27)$$

Likewise Q^m is a vector of equivalent nodal charges

$$Q^m = \frac{\partial W}{\partial \phi^m} = \int_s q^s N_4(x_i) ds \qquad (3.28)$$

Kinematic conditions and conditions on the electric potential are imposed directly on the nodal values, which then can be eliminated from further analysis.

The volume integration of the shape functions is carried out element by element. The contributions from one element are called the element stiffness- and mass matrix. The total stiffness matrix and mass matrix are hence sums of element matrices. The integration over each element is normally performed in a local coordinate system, which is related to the (local) nodes of the actual element. The elements are defined by the mapping of the local nodes on a subset of the global nodes.

Finite elements are classified by the shape of the element, the number of (local) nodes and the classes of the shape functions. Various types of elements have been employed for calculations on piezoelectric materials. In the case of low electro-mechanical coupling (as in Quartz) purely elastic calculations may be sufficient [39,40,41] and common general purpose finite element computer programs may be used. For materials with higher electro-mechanical coupling the piezoelectric effect must be incorporated. This can be done in just as many different ways as in the elastic case. Kagawa and Yamabuchi have developed a triangular axisymmetric element, where the electric field is given by one global degree of freedom [42]. They have also developed a two-dimensional triangular element where the piezoelectric effect is fully included [43]. The first to fully include the piezoelectric effect in finite elements were Allik and Hughes [19]. They developed a three-dimensional element of shape of a tetrahedron. If the geometric coordinates are interpolated by the same shape functions as the displacements and the electric field, the element is called isoparametric [21]. As the mechanical characteristics are more important than the electrical in most problems, the cost of including the electrical degrees of freedom may be reduced by introducing them as a pertubation of the elastic solution [44]. If the piezoelectric constants e_{42} and e_{51} can be ignored, the piezoelectric effect may be added to existing finite element programs by simple matrix manipulation [45]. This requirement is approximately fulfilled for thickness vibrations of plates and radially poled spheres and cylinders, but not for shear wave transducers.

4. THE FINITE ELEMENT METHOD WITH AXISYMMETRIC PIEZOELECTRIC ELEMENTS

Three-dimensional harmonic analysis of piezoelectric ultrasonic transducers by use of the finite element method demands solution of very large systems of equations. The number of nodes is large,

because the elements must be small compared with any characteristic wavelength as well as any geometric length scale. The bandwidth becomes large because of large connectivity. In comparison with purely elastic analysis there is one extra degree of freedom (the electric potential) in each node.

For this reason it was decided to restrict the attention to the axisymmetric case, which still applies to a large number of ultrasonic transducers. The axisymmetric element used by Kagawa [42] have only a single global electrical degree of freedom, a constant electric field with an axial component only. From the solution for an infinite plate in Section 2.1 this is known not be sufficient, especially not near resonance. Furthermore, there are restrictions on the orientation of the elements. As no other axisymmetric and fully piezoelectric finite elements were known, it was decided to develop one. The choice fell on the simple linear triangular ring with nodes in the corners. The element was developed as an extension of the corresponding elastic element given by Krenk [46]. This element has the advantages of having explicit expressions for the stiffness and mass matrix and of having no restrictions with respect to shape, orientation or placement.

In the axisymmetric case the Lagrangian is

$$L = \pi \int_A (- \omega^2 \rho u_\alpha u_\alpha + S_p C_{pq} S_q - 2E_\alpha e_{\alpha p} S_p - E_\alpha \varepsilon_{\alpha\beta} E_\beta) x_1 \, dA \tag{4.1}$$

The Lagrangian is approximated by inserting the displacements and the electric potential in terms of their nodal values and a set of shape functions. When the shape functions are linear, the electric field and the components of the strain tensor, except S_2, become constant. To perform the integration in (4.1) it is necessary to integrate constants, S_2, S_2 squared, and $u_\alpha u_\alpha$. Formulas for these terms, integrated over a single element, can be expressed explicitly. They will be derived in the next section.

4.1. The element integrals

The desired integration formulas are conveniently found by employing triangular area coordinates λ_i. Let a triangle of area A be given by the coordinates of its corners (nodes) x_α^i

$$\ell_\alpha{}^i = x_\alpha^{i-1} - x_\alpha^{i+1} \tag{4.2}$$

where the superscripts must be interpreted as being modulus 3 on the numbers 1,2,3. If the area of the triangle, which has x_α as one of its corners and ℓ_α^i as base line, is denoted by A^i, the area coordinates to x_α become

$$\lambda^i = \frac{A^i}{A} \tag{4.3}$$

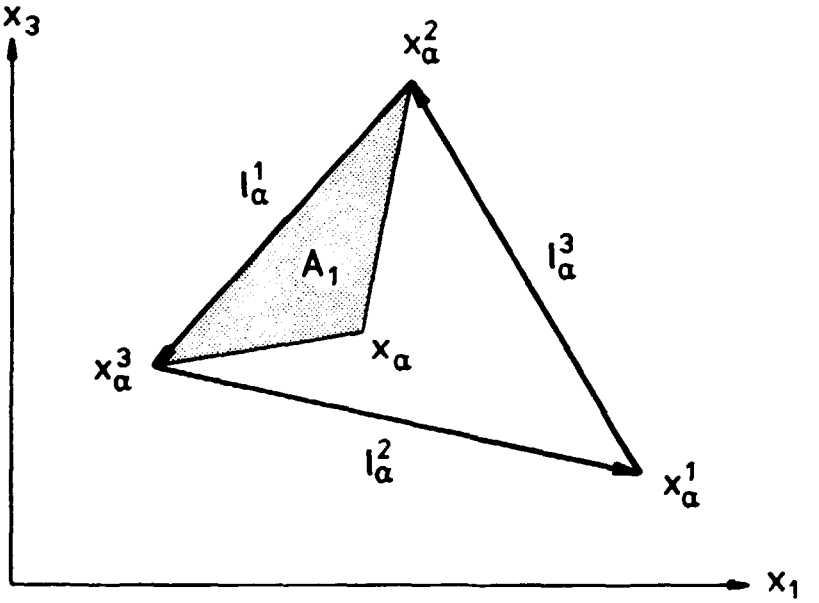

Fig. 4.1. Triangular area coordinates.

It follows immediately that the three area coordinates must sum up to unity. The area coordinates also are equal to the weights to be given to the nodal values in linear interpolation. As the cartesian coordinates also vary linearly and may be found by interpolation between the nodes, we get

$$x_\alpha = \lambda^i x_\alpha^i \tag{4.4}$$

and

$$\begin{aligned} u_\alpha &= \lambda^i u_\alpha^i \\ \phi &= \lambda^i \phi^i \end{aligned} \tag{4.5}$$

The change in the areas A^i, for a small change in x_α, dx_α, equals the dot product between dx_α and the normal vector to the base line. This is why the partial derivatives of λ^i are

$$\lambda^i{}_{,\alpha} = \frac{n_\alpha^i}{2A} \tag{4.6}$$

where n_α^i is the positive normal to ℓ_α^i.

$$\begin{aligned} n_1^i &= -\ell_3^i \\ n_3^i &= \ell_1^i \end{aligned} \tag{4.7}$$

The strain vector and the electric field vector are - in area coordinates - found by substituting (4.5) into their definitions (2.23), (2.24). The chain rule and (4.6) are then used to give

$$\begin{aligned} S_1 &= \frac{-1}{2A} \quad \ell_3^i u_1^i \\ S_2 &= \frac{\lambda^i u_1^i}{\lambda^j x_1^j} \\ S_3 &= \frac{1}{2A} \quad \ell_1^i u_3^i \\ S_5 &= \frac{}{2A} \; (\ell_1^i u_1^i - \ell_3^i u^i{}_3) \end{aligned} \tag{4.8}$$

and

$$E_1 = \frac{1}{2A} \quad \ell_3^i \phi^i$$

$$E_3 = \frac{-1}{2A} \quad \ell_1^i \phi^i \tag{4.9}$$

Most of the integrals are directly found from the formulas for powers of λ^i integrated over the entire element.

$$\int_A (\lambda^1)^r (\lambda^2)^s (\lambda^3)^t \, dA = 2A \, \frac{r!s!t!}{(r+s+t+2)!} \tag{4.10}$$

This gives the formula for integration of the constants

$$\int_A x_1 \, dA = \int_A \lambda^i x_1^i \, dA = A \, x_1^e \tag{4.11}$$

where the superscript e on x_1^e denotes the average of the nodal values of x_1. The formula for integration of s_2 is very similar

$$\int_A S_2 \, x_1 \, dA = \int_A \lambda^i u_1^i \, dA = A \, u_1^e \tag{4.12}$$

The integral of S_2 squared is more complicated, and is first re-written as

$$\int_A s_2^2 \, x_1 \, dA = \int_A \frac{u_1^i \lambda^i \lambda^j u_1^j}{\lambda^k x_1^k} \, dA = u_1^i J^{ij} u_1^j \tag{4.13}$$

where

$$J^{ij} \equiv \int_A \frac{\lambda^i \lambda^j}{\lambda^k x_1^k} \, dA \quad ; \qquad J_n^i \equiv \int_A \frac{(\lambda^i)^n}{\lambda^k x_1^k} \, dA \tag{4.14}$$

From the definition (4.14) it is obvious that $J^{ij} = J_2^i$ for $i = j$. J_n^i is given in [46]

$$J_n^i = \frac{2A}{\ell_1^i}\left[\frac{1}{n+1} F_n(y)\right] \quad \begin{matrix} y = x_1^i/x_1^{i+1} - 1 \\ y = x_1^i/x_1^{i-1} - 1 \end{matrix} \tag{4.15}$$

where

$$F_n(y) = \frac{1}{(-y)^{n+1}}\left\{\ln(1+y) - \sum_{m=1}^{n} \frac{1}{m}(-y)^m\right\} \tag{4.16}$$

The mixed terms, $J^{ij}(i \neq j)$ can be expressed by the unmixed. At least one of the quantities ℓ_1^i and ℓ_1^j must be different from zero. If ℓ_1^i is numerically largest then that is chosen and the defining Equation (4.14) is multiplied with it. After a bit of manipulation the following equation is obtained:

$$e_{ijk}\ell_1^i J^{ij} = \frac{A}{3} - x_1^k J_1^j + e_{ijk}\ell_1^i J_2^j; \text{ no sums} \tag{4.17}$$

where i,j, and k all are different and e_{ijk} is the permutation symbol. The alternative equation (if ℓ_1^j was smallest) is obtained by interchanging i and j. Special cases arise when one side is parallel to the axis, or one or two corners are located on the axis. They can all be handled by limit processes and are treated in [46].

The final integral is

$$\int_A u_\alpha u_\alpha x_1 dA = u_\alpha^i u_\alpha^i x_1^k \int_A \lambda^i\lambda^j\lambda^k dA \tag{4.18}$$

$$= u_\alpha^i u_\alpha^i x^k \frac{A}{60}\left\{1 + (\delta_{ij} + \delta_{jk} + \delta_{ik}) + 2\delta_{ijk}\right\}$$

where δ_{ijk} is unity if $i = j = k$, otherwise zero. The result follows directly from the integration formula (4.10). The expression in braces is symmetric with respect to i,j, and k but as the remaining equation is symmetric in only i and j, it may as well be

factorized as $(1 + \delta_{ij})(1 + \delta_{ik} + \delta_{jk})$ if the summation convention is suspended.

4.2. The element matrices

The element matrices are obtained by substituting the approximate strain vector (4.8) and electric field vector (4.9) into the Lagrangian (4.1). The integration area, A is the crosssection of the actual element only. The integration is performed with the aid of the integration formulas from the previous section. The element matrices are obtained by taking the second-order partial derivatives (3.26). For ω equal to zero the generalized element stiffness matrix is obtained

$$K_{11}^{ij} = \frac{V}{4A^2}\{C_{11}\ell_3^i\ell_3^j + C_{55}\ell_1^i\ell_1^j\} - \frac{\pi}{3}C_{12}(\ell_3^i + \ell_3^j) + 2\pi C_{11}J^{ij}$$

$$K_{13}^{ij} = \frac{V}{4A^2}\{C_{13}\ell_3^i\ell_1^j + C_{55}\ell_1^i\ell_3^j\} - \frac{\pi}{3}C_{13}\ell_1^j \qquad (4.19)$$

$$K_{14}^{ij} = \frac{V}{4A^2}\{C_{31}\ell_3^i\ell_1^j + e_{15}\ell_1^i\ell_3^j\} - \frac{\pi}{3}e_{31}\ell_1^j$$

$$K_{33}^{ij} = \frac{V}{4A^2}\{C_{55}\ell_3^i\ell_3^j + C_{33}\ell_1^i\ell_1^j\}$$

$$K_{34}^{ij} = \frac{V}{4A^2}\{e_{15}\ell_3^i\ell_3^j + e_{33}\ell_1^i\ell_1^j\}$$

$$K_{44}^{ij} = \frac{V}{4A^2}\{\varepsilon_{11}\ell_3^i\ell_3^j + \varepsilon_{33}\ell_1^i\ell_1^j\}$$

The element mass matrix is the part that is proportional to ω^2; it is found directly from (4.18)

$$M_{\alpha\beta}^{ij} = \delta_{\alpha\beta} \frac{\pi\rho A}{30} x_1^k (1 + (\delta_{ij} + \delta_{ik} + \delta_{jk}) + 2\delta_{ijk})$$

$$= \delta_{\alpha\beta} (1 + \delta_{ij}) \frac{\pi\rho A}{30} (x_1^i + x_1^j + 3x_1^e) \tag{4.20}$$

The element matrices are added to give the global matrices which have the same structure as the element matrices except that the superscripts, (now n,m) refer to global node numbers. The (global) nodal values are connected by the equation

$$\begin{Bmatrix} K_{11}^{mn} & K_{13}^{mn} & K_{14}^{mn} \\ K_{31}^{mn} & K_{33}^{mn} & K_{34}^{mn} \\ K_{44}^{mn} & K_{43}^{mn} & K_{44}^{mn} \end{Bmatrix} - \omega^2 \begin{Bmatrix} M_{11}^{mn} & 0 & 0 \\ 0 & M_{33}^{mn} & 0 \\ 0 & 0 & 0 \end{Bmatrix} \begin{Bmatrix} u_1^n \\ u_3^n \\ \phi^n \end{Bmatrix} = \begin{Bmatrix} F_1^m \\ F_3^m \\ -Q^m \end{Bmatrix} \tag{4.21}$$

This equation is of the same form as in purely elastic finite element analysis, except that the mass matrix contains zeros in the diagonal. This is because the quasistatic approximation has been used for the electric field. (4.21) can be used for a forced-response analysis in which case the frequency ω is fixed. The stiffness and the mass matrices are then combined to one dynamic stiffness matrix $D = K - \omega^2 M$. (4.21) can also be used for an eigenfrequency analysis. The first step is then to invert the mass matrix and the zeros in the diagonal will then give problems. The problems may be overcome simply by assigning small values to the zero elements in the diagonal. This introduces false eigenfrequencies, but they can be placed outside the frequency range of interest by making the diagonal values small enough. It is also possible to eliminate the electrical degrees of freedom before solving the eigenvalue problem [47]. Prescribed displacements or electric potential allows elimination of the degrees of freedom. Prescribed stress or electric charge are integrated into equivalent nodal forces and charges (3.17), (3.28).

4.3. Damping in finite elements

In many applications of the finite element method, damping is only of little interest, but in dynamics it is generally important. For ultrasonic transducers damping and its influence on the frequency characteristics is an important design parameter. Many transducers have a highly damping material attached to the back of the piezoelectric element to get a wider frequency range and a shorter impulse response. Damping has many origins, but the knowledge of these is generally inaccurate, and a very detailed modelling of the damping is pointless. Emphasis is instead put on simplicity.

Two kinds of internal damping are commonly used: If the reaction force is proportional to the relative velocity of the different parts of the body, the damping is called viscous. In harmonic analysis this corresponds to a damping which is proportional to the frequency. If the damping is independent of the frequency, it is called hysteretic. The following discussion only cover the mechanical damping, but is easily extented to electrical damping simply by thinking of displacements as generalized, i.e. to cover both displacements and electric potential and generalized forces to cover both mechanical forces and electric charge. The electric losses in a resistor are then viscous.

Damping may be included in the finite element equation by introducing a damping matrix $C_{\alpha\beta}^{mn}$ in the equation as

$$(K_{\alpha\beta}^{mn} - i\omega^{\gamma}C_{\alpha\beta}^{mn} - i\omega^{2}M_{\alpha\beta}^{mn})\ u_{\beta}^{n} = F_{\alpha}^{m} \qquad (4.22)$$

γ is called the frequency exponent. $\gamma = 1$ corresponds to viscous damping and $\gamma = 0$ to hysteretic damping. Hysteretic damping has been included in the actual elements by assigning complex values to the stiffness constants C_{pq} and the dielectric constants $\varepsilon_{\alpha\beta}$. The cost of including damping in a forced response analysis is that the system of equations become complex. If damping is included in eigenfrequency analysis the "size" of the problem is furthermore doubled [48], unless the damping matrix is a linear combination of the stiffness- and the massmatrices

$$C_{\alpha\beta}^{mn} = aK_{\alpha\beta}^{mn} + bM_{\alpha\beta}^{mn} \tag{4.23}$$

For viscous damping is this called Rayleigh damping. In this case the damping matrix can be eliminated by substituting (4.23) into (4.22). Premultiplication with $((1-i\omega^{\gamma}a)M_{\alpha\beta}^{mn})^{-1}$ then gives

$$\left\{(M_{\alpha\beta}^{mn})^{-1}K_{\alpha\beta}^{mn} - \frac{i\omega^{\gamma}b - \omega^2}{1-i\omega^{\gamma}a}I_{\alpha\beta}^{mn}\right\} u_{\beta}^{n} = 0 \tag{4.24}$$

where $I_{\alpha\beta}^{mn} = \delta_{\alpha\beta}\delta_{mn}$ is the identity matrix. (4.24) is in the form of the standard eigenvalue problem.

The internal damping causes vibrations to have finite amplitudes even at resonance and propagating waves to be attenuated. For piezoelectric materials is it common to represent internal losses by loss tangents [49, p. 84]. The complex material data are then obtained by multiplying the real part with the factor $(1-i\tan\delta)$ where $\tan\delta$ is the loss tangent. If the losses instead are given by the attenuation of a propagating wave

$$u = u_o e^{ikx} \tag{4.25}$$

the complex wave number is given by

$$k = \omega/c + i\alpha(\omega) \tag{4.26}$$

where $\alpha(\omega)$ is the frequency dependent attenuation (in neper/m) [50]. The stiffness constant for the actual wave, f.x. C_{1111} can then be given by

$$C_{1111} = \rho\frac{\omega^2}{k^2} = \rho c^2\left(1+i\frac{\alpha(\omega)c}{\omega}\right)^{-2} \tag{4.27}$$

5. ACOUSTIC RADIATION

In a realistic situation a transducer will be used to radiate or measure ultrasound into or from a medium. This raises two questions: "How does the radiated field look?", and "How does the presence of the medium influence the vibrations of the transducer?" Both questions could be answered by including the medium in a finite element calculation, but this is impractical, as the volume of the medium normally is orders of magnitude larger than the transducer. Instead the medium is represented by a half-space, and for simplicity it is assumed to consist of an invicid fluid.

In acoustics it is common practice to use the velocity, $v_i = \dot{u}_i$, and pressure, $p = -1/3T_{ii}$, as primary variables, both of which are derived from the scalar velocity potential ψ.

$$p = \rho\dot{\psi} \tag{5.1}$$

$$v_i = -\psi_{,i} \tag{5.2}$$

where ρ is the mass density. The potential must satisfy the wave equation

$$\psi_{,ii} = \frac{1}{c_p^2}\ddot{\psi} \tag{5.3}$$

where c_p is the speed of sound in the fluid. When only time harmonic variation is considered, the wave equation degenerates to the Helmholtz equation

$$\psi_{,ii} + k^2\psi = 0 \tag{5.3b}$$

where k is the wave number ω/c_p. ψ can be represented within a volume V by an integral over its surface [13, § 293]

$$\psi(x_i) = \frac{1}{4\pi}\int_S \left\{\psi(\xi_i),_j n_j \frac{e^{ikr}}{r} - \psi(\xi_i)\left(\frac{e^{ikr}}{r}\right),_j n_j\right\} dS \tag{5.4}$$

This representation is known as Helmholtz's formula. r is the distance between the "observation" point x_i and the "source" point ξ_i i.e. $r = |\xi_i - x_i|$. As both ψ and its normal derivative must be known on the surface, Helmholtz's formula rarely will provide explicit solutions for ψ. In the case of a half-space it will, however, prove useful. Consider a half-space $x_3 > 0$ with the surface $S(x_3 = 0)$ and outward unit normal vector $n_i = -\delta i_3$. If ψ is extended symmetrically into the other half-space, the contribution from ψ will vanish, because the unit normal in $x_3 < 0$ has the opposite orientation. On the other hand, the contribution from the normal derivative is doubled. The potential in the half-space then becomes

$$\psi(x_i) = \frac{1}{2\pi} \int_S v_3(\xi_i) \frac{e^{ikr}}{r} dS \qquad (5.5)$$

This shows that ψ can be found if the normal velocity is prescribed on the surface. If ψ had been extended antisymmetrically, an equation, which gives ψ from prescribed surface pressure, would have been obtained.

5.1. Generalized acoustic impedance

The influence of the loading of the transducer is due to the pressure from the surrounding medium on the surface of the transducer. As both the pressure and the velocity are axisymmetrically distributed, the surface pressure can be written

$$p^o(x_1) = \frac{-i\omega\rho}{2\pi} \int_0^{2\pi} \int_0^{\infty} v_3^o(\xi) \frac{e^{ikr}}{r} \xi \, d\xi \, d\theta \qquad (5.6)$$

where v_3^o is the velocity on the surface of the half space, and $r = (x_1^2 + \xi^2 - 2x_1\xi\cos\theta)^{1/2}$. If v_3^o is constant over S, p^o will also be constant, and need only to be calculated at a single point, most conveniently $x_1 = 0$. This leads to $p^o = \rho c v_3^o$. The product ρc is called the specific acoustic impedance of a fluid, mainly due to this result.

The so-called baffled piston problem is also covered by (5.6), if v_3^o is prescribed to be zero for $\xi > a$ and to have a constant value over the disk $\xi < a$. The piston impedance Z is the ratio of the total force on the piston to the velocity of the piston. It is given by the double-area-integral

$$Z = \frac{-i\omega\rho}{2\pi} \int_S \int_S \frac{e^{ikr}}{r} \, dS_\xi \, dS_x \tag{5.7}$$

This integral was calculated by Rayleigh [13, § 302]. It can be divided into two integrals. One for $x > \xi$ and the other for $x < \xi$. Due to the symmetry in x and ξ, these integrals give equal contributions. This is why the impedance becomes

$$Z = -2i\omega\rho \int_0^a \int_{A_x} \frac{e^{ikr}}{r} \, dA \, x \, dx \tag{5.8}$$

where A_x is the disk with radius x. The area integral with the observation point, x_i, on the edge of the disk can be calculated as

$$\int_{-\frac{\pi}{2}}^{\frac{\pi}{2}} \int_0^{2x\cos\theta} \frac{e^{ikr}}{r} \, r \, dr \, d\theta = \frac{-\pi}{ik} \left(1 - J_o(2kx) + iH_o(2kx)\right) \tag{5.9}$$

where $J_o()$ is the Bessel function, and H_o the Struve function of zero order. With this result substituted into (5.8), the impedance can be found by use of elementary relations for Bessel and Struve functions [51, 9.1.29, 12.1.12 ($\nu = 1$)].

$$Z = \rho c \, A \left\{ \left(1 - \frac{J_1(2ka)}{ka}\right) - i \frac{H_1(2ka)}{ka} \right\} \tag{5.10}$$

A is the area of the piston, πa^2. Greenspan [17] has extended this result by also calculating the impedance for Gaussian and polynomial velocity distributions, the latter of the form $v_3^o(x_1) = (1 - x_1^2/a^2)^n$; $n = 0,1,2$. This does not, however, provide any information about the distribution of the reaction force. To obtain this, both the normal velocity and the pressure are expanded

in orthogonal series, here chosen to be polynomials, which leads to Legendre polynomials in a form first used by Zernike [52]

$$p^o(x_1) = p_n P_n(1 - 2x_1^2/a^2) \; ; \; n = 1,2,...$$
$$v_3^o(x_1) = v_n P_n(1 - 2x_1^2/a^2) \; ; \; n = 1,2,... \tag{5.11}$$

$P_n()$ is the Legendre polynomial of degree n. The expansion coefficients follow from the orthogonality relation of the Legendre polynomials.

$$p_n = (2n+1)\frac{2}{a^2}\int_o^a p^o(x_1)P_n(1-2x_1^2/a^2)\, x_1\, dx_1$$
$$v_n = (2n+1)\frac{2}{a^2}\int_o^a v_3^o(x_1)P_n(1-2x_1^2/a^2)\, x_1\, dx_1 \tag{5.12}$$

The relation between the expansion coefficients is found by substituting the expansions into (5.6). Subsequent use of the orthogonality relations gives

$$p_m = -2i\,\rho c\,(2m+1)\, Z_{mn}\, v_n \tag{5.13}$$

where Z_{mn} will be called the generalized impedance matrix (for the Legendre polynomial expansion) and is given by

$$Z_{mn} = \frac{k^2}{2\pi a^2}\int_o^{2\pi}\int_o^a\int_o^a P_m(1-2x_1^2/a^2)P_n(1-2\xi^2/a^2)\,\frac{e^{ikr}}{kr}\,\xi d\xi\, x_1 dx_1 d\theta \tag{5.14}$$

where $r = (x_1^2 + \xi^2 - 2x_1\xi\cos\theta)^{1/2}$ is the distance between the source and "receiver" points. The exponential factor e^{ikr}/kr is Green's function for the wave equation in three dimensions. It can be shown to be the zero-order Hankel transform of $(x^2-1)^{1/2}$. This result is sometimes called Lamb's integral [17]. The Bessel function in the Hankel transform can be represented by a Fourier series [53] by Neumann's summation theorem. The angular integral in (5.14) then leaves only the first term. Altogether this leads to

$$\frac{1}{2\pi}\int_0^{2\pi}\frac{e^{ikr}}{kr}\,d\theta = \frac{1}{2\pi}\int_0^{2\pi}\int_0^{\infty}\frac{J_0(krs)}{(s^2-1)^{1/2}}\,sds\,d\theta$$

$$= \int_0^{\infty}\frac{J_0(kx_1s)J_0(k\xi s)}{(s^2-1)^{1/2}}\,sds \qquad (5.15)$$

This formula can be used to replace the angular integral in (5.14) with an infinite integral, but the Bessel functions are now functions of x_1 and ξ and can be combined with the Legendre polynomials into known Hankel transforms ([54] formula 7.251). The generalized impedance matrix then takes the form of a single infinite integral

$$z_{mn} = \int_0^{\infty}\frac{J_{2m+1}(kas)J_{2n+1}(kas)}{s(s^2-1)^{1/2}}\,ds \qquad (5.16)$$

Direct numerical evaluation of (5.16) is difficult due to the oscillatory behaviour of the integrand. It may, however, be transformed to a finite integral by use of contour integration in the complex plane followed by a trigonometric substitution (see Appendix B)

$$z_{mn} = -i\int_0^{\frac{\pi}{2}}\Big\{J_{2m+1}(ka\sin\theta)H^{(2)}_{2n+1}(ka\sin\theta) - (-1)^{m-n}\frac{2i}{\pi}I_{2m+1}(ka\tan\theta)K_{2n+1}(ka\tan\theta)\Big\}\frac{d\theta}{\sin\theta} \qquad (5.17)$$

$H^{(2)}_{\nu}()$ is the Hankel function of order ν. $I_{\nu}()$ and $K_{\nu}()$ are the modified Bessel functions. It may be noted that the integrand is not singular at $\theta = 0$.

5.2. Matching to finite element model

The velocity of the surface of the transducer is determined by the velocities of the nodes on its surface - $i\omega\, u_3^m$, and the shape functions on the surface, N_m^o

$$v_3^o(x_1) = - i\omega\, u_3^m\, N_m^o(x_1) \tag{5.18}$$

The implied summation is assumed to be carried out for all the nodes on the surface. The polynomial velocity distribution on the surface of the half-space is matched to that of the transducer by the method of least squares. The expansion coefficients are given in the form

$$v_n = - i\omega\, L_{nm}\, u_3^m \tag{5.19}$$

The method of least squares is equivalent to use of the orthogonality relation for the Legendre polynomials. L_{nm} can therefore be found by substituting the interpolated normal velocity (5.18) into (5.12).

$$L_{nm} = (2n+1)\,\frac{2}{a^2}\int_o^a N_m^o(x_1) P_n(1-2x_1^2/a^2)\, x_1 dx_1 \tag{5.20}$$

The nodal forces are the integrals of the pressure, with the shape functions as weight functions (3.27). Their relation to the expansion coefficients of the pressure is found by substituting the expansion (5.11) into (3.27). The relation can be written in a form similar to the relation between velocities and their expansion coefficients

$$F_3^m = \sum_n \frac{A}{2n+1}\, L_{mn} p_n \tag{5.21}$$

The expansion coefficients are now eliminated from (5.13) with (5.19) and (5.21), to give the stiffness matrix for the half-space boundary element

$$K_{mn} = -2\omega \rho c A L_{mr} Z_{rs} L_{sn} \tag{5.22}$$

m and n denotes the nodes on the interface between the transducer and the half-space. The implied summation over r and s runs up to where Z_{rs} is truncated. This is determined by the required degree of the matching Legendre polynomials.

Such methods of combining finite element models, with wave representations in the surrounding medium is sometimes referred to as global-local finite element methods [55].

5.3. The radiated field

A finite element analysis with the half-space stiffness matrix included, provides the nodal normal displacements u_3^m, from which the expansion coefficients of the normal velocity is found by use of (5.19). It is then possible to derive closed form expressions for the pressure in certain special cases.

The pressure on the surface is immediately obtained from the impedance matrix as

$$p^o(x_1) = -2i\rho c \sum_m (2m+1) P_m(1-2x_1^2/a^2) Z_{mn} v_n \tag{5.23}$$

The farfield is found by the well known far-field approximation, whereby the field becomes proportional to the two dimensional Fourier transform of the velocity distribution. As the velocity distribution is axisymmetric the two-dimensional Fourier transform can be reduced to the Hankel transform of zero order. Consider a point P located at a distance R from the center C of the circular disk. Let the angle between the axis of the disk and the line CP be θ. Let P' be the projection of P onto the plane of the disk. The actual source point is Q the distance $|CQ| = \xi$ and the angle P'CQ is ϕ.

For $R >> \xi$ i.e. in the far-field the distance $|PQ| = r$ can be approximated by

$$r = \sqrt{R^2 + \xi^2 - 2R\xi\cos\phi\sin\theta} \tag{5.24a}$$

$$\cong R + \xi\cos\phi\sin\theta \tag{5.24b}$$

$$\cong R \tag{5.24c}$$

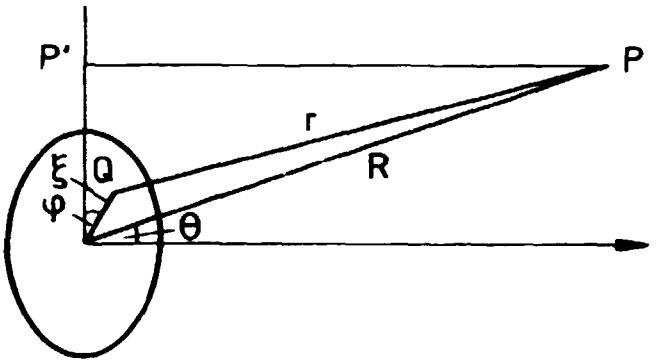

Fig. 5.1. Geometry of the far-field problem.

In the far-field approximation (5.24b) is substituted into the phase term, e^{ikr}, and (5.24c) is substituted into the geometric damping term, r^{-1} in (5.5). This gives

$$p(x_\alpha) \cong \frac{-i\omega\rho}{2\pi}\frac{e^{ikR}}{R}\int_o^a\int_o^{2\pi} v_3^o(\xi)e^{-ik\xi\cos\phi\sin\theta}\,d\phi\,\xi d\xi$$

$$\cong -i\omega\rho\frac{e^{ikR}}{R}\int_o^a v_3^o(\xi)J_o(k\xi\sin\theta)\xi d\xi \tag{5.25}$$

When the expression for $v_3^o(\xi)$, (5.11) is inserted in (5.25) the Hankel transform of Legendre polynomials can be used to get [54, formula 7.251].

$$p(x_\alpha) \cong -i\rho c(ka^2)\frac{e^{ikR}}{kR}\sum_n (-1)^n v_n \frac{J_{2n+1}(ka\sin\theta)}{ka\sin\theta} \tag{5.26}$$

where $R^2 = x_\alpha x_\alpha$ and $R\sin\theta = x_1$. The first term corresponds to a rigid piston and can be found in any standard text [1, p 63]. The far-field from polynomial velocity distributions which approximately corresponds to simply supported and clamped circular disks have been found by Dekker, Piziali, and Dong [16], but as they have not used orthogonal polynomials their expressions differ from the expressions above. They express the result by use of the Bessel functions of order zero and one only. (5.26) is easily rewritten to that form by use of the recurrence relations. If the transducer were focused these relations would have been valid not in the far-field but in the focal distance [15,18]. The first four terms in (5.26) are shown in Fig. 5.2.

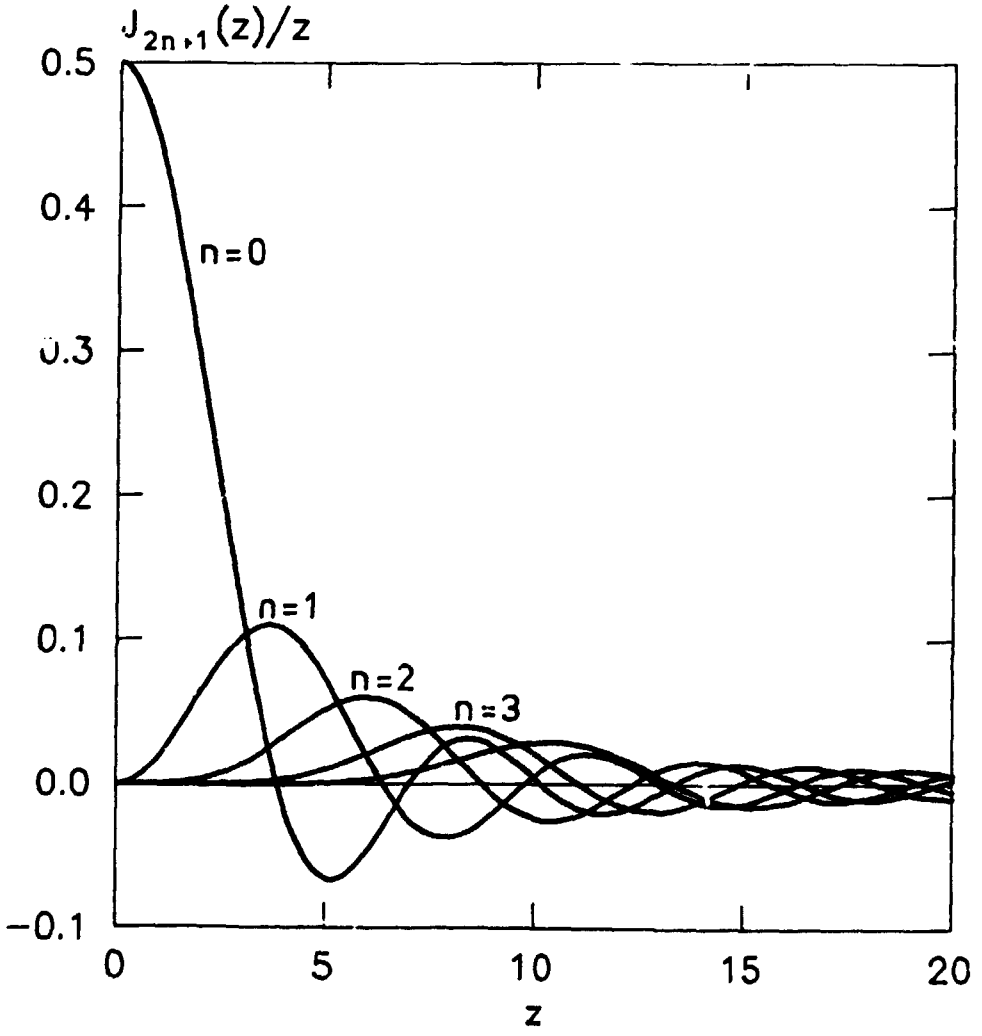

Fig. 5.2. Far-field from the first four terms in the Legendre polynomial expansion of the normal velocity (5.11) as given in (5.26). $z = ka\sin\theta$.

On the axis the distance to the source point is independent of the angular coordinate of the source point. $r = (\xi^2+x_3^2)^{1/2}$. The expression for the pressure then simplifies to

$$p(x_\alpha)\Big|_{x_1=0} = -i\omega\rho \int_0^a v_n P_n(1-2\xi/a^2) \frac{e^{ik\sqrt{\xi^2+x_3^2}}}{\sqrt{\xi^2+x_3^2}} \xi d\xi \qquad (5.27)$$

The substitution $s = \sqrt{\xi^2+x_3^2}$ would lead to integrals with polynomials in s^2 multiplied by e^{iks}. Each term could then be integrated by repeated use of partial integration. It is also possible to take the advantage of the characteristics of the Legendre polynomials. If the substitution $\cos\psi = 1 - 2\xi^2/a^2$ is made and $y_\pm = 1/2((x_3^2+a^2)^{1/2} \pm x_3)$ introduced, (5.27) is then written as

$$p(x_\alpha)\Big|_{x_1=0} = \frac{-i\omega\rho a^2}{4} \int_0^\pi v_n P_n(\cos\psi) \frac{e^{ik(y_+^2+y_-^2-2y_+y_-\cos\psi)^{1/2}}}{k(y_+^2+y_-^2-2y_+y_-\cos\psi)^{1/2}} \sin\psi d\psi \qquad (5.28)$$

This can be recognized as being equivalent to the field from a sphere of radius y_- in a distance of y_+ [53, p. 367 with $\gamma = 1/2$)]. This analogy can be extented to focusing transducers as pointed out by Krenk [18], who also explains the analogy in greater detail. By this analogy the pressure on the axis becomes

$$p(x_\alpha)\Big|_{x_1=0} = \frac{1}{2} \rho c (ka)^2 \sum_n v_n j_n(ky_-) h_n^{(1)}(ky_+) \qquad (5.29)$$

Where $j_n(\ )$ and $h_n^{(1)}(\ )$ are the spherical Bessel and Hankel functions, respectively. The numerical value of the first terms in (5.29) are shown in Fig. 5.3 for ka = 20.

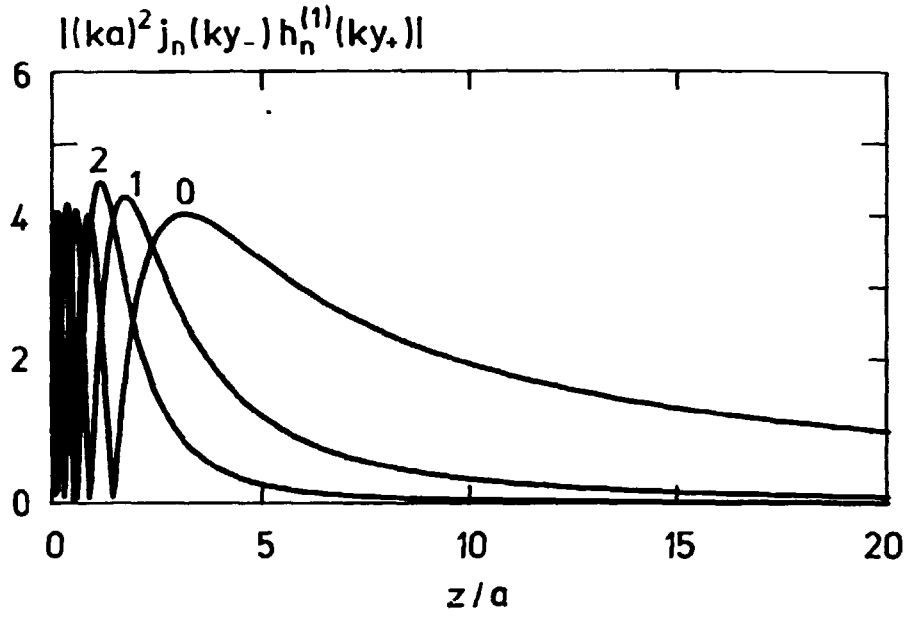

Fig. 5.3. Amplitude of the pressure on the axis from the first three terms of the polynomial expansion of the velocity distribution (5.29) for ka = 20.

6. FINITE ELEMENT ANALYSIS OF CYLINDRICAL STRUCTURES

In finite element analysis of ultrasonic transducers the required element size is determined by the wavelength, rather than the geometry of the transducer. Even a simple structure, such as a cylinder, must be divided into a large number of finite elements. The element model can be made as a sequence of identical layers. If the boundary conditions along the generating lines furthermore are constant (or periodic), they may be incorporated in the equation for each layer, and the equations will still be identical. This may be utilized in an efficient stacking procedure for making super elements of finite cylindrical substructures, or to analyse infinite waveguides.

6.1. Super elements for cylindrical substructures

A super element is an assemblage of finite elements which is treated as a single element. Nodes in a super element which never are shared with other super elements are called internal. The other nodes are external. Normally the nodes located on the surface of an element are external, but in the present case only nodes on the interface between different layers are external.

The internal nodes may be eliminated prior to the use of a super element. When nodes are eliminated the simple structure of the equation of motion, with only a stiffness and a mass matrix is spoiled. This means that the elimination can be done only when the frequency has been chosen. It is then easier to work with the dynamic stiffness matrix, D, which is a combination of the stiffness and the mass matrices. The dynamic stiffness matrix for a single layer may be written in matrix notation in partitioned form as

$$\begin{Bmatrix} D_{ee} & D_{ei} \\ D_{ie} & D_{ii} \end{Bmatrix} = \begin{Bmatrix} K_{ee} & K_{ei} \\ K_{ie} & K_{ii} \end{Bmatrix} - \omega^2 \begin{Bmatrix} M_{ee} & M_{ei} \\ M_{ie} & M_{ii} \end{Bmatrix} \tag{6.1}$$

where the indices e and i refer external and internal nodes, respectively. The equation of motion is then

$$\begin{Bmatrix} D_{ee} & D_{ei} \\ D_{ie} & D_{ii} \end{Bmatrix} \begin{Bmatrix} u_e \\ u_i \end{Bmatrix} = \begin{Bmatrix} f_e \\ f_i \end{Bmatrix} \tag{6.2}$$

where u_e (u_i) is a vector of all external (internal) degrees of freedom. The lower part of (6.2) gives u_i in terms of u_e and f_i. When this is substituted into the upper part the condensed equation is obtained.

$$\{D_{ee} - D_{ei}(D_{ii})^{-1}D_{ie}\}\{u_e\} = f_e - D_{ei}(D_{ii})^{-1}f_i \tag{6.3}$$

(6.3) gives the dynamic stiffness matrix for a single layer super element. f_i would often be zero. The layers will have nodes on only their two faces. The dynamic stiffness matrix in (6.3) may

be partitioned with respect to the two sides. Two layers may be combined to give

$$\begin{Bmatrix} D_{11} & D_{12} & 0 \\ D_{21} & D_{22}+D_{11} & D_{12} \\ 0 & D_{21} & D_{22} \end{Bmatrix} \begin{Bmatrix} u_{n-1} \\ u_n \\ u_{n+1} \end{Bmatrix} = \begin{Bmatrix} f_{n-1} \\ f_n \\ f_{n+1} \end{Bmatrix} \tag{6.5}$$

where the indices on the displacements, u_n and the nodal forces f_n, refer to the interface number

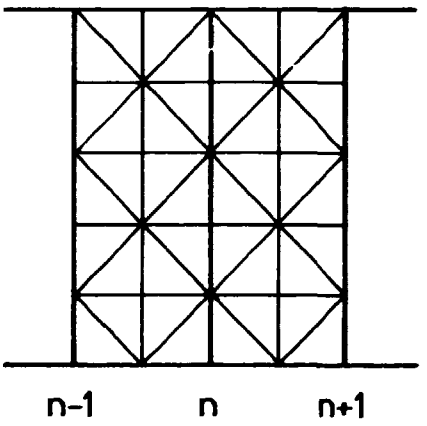

Fig. 6.1. Sequence of identical super elements for modelling cylinders.

The nodes on their common interface are internal. Condensation of 6.5 gives

$$\begin{Bmatrix} D_{11}-D_{12}(D_{11}+D_{22})^{-1}D_{21} & D_{12}(D_{11}+D_{22})^{-1}D_{12} \\ D_{21}(D_{11}+D_{22})^{-1}D_{21} & D_{22}-D_{21}(D_{11}+D_{22})D_{12} \end{Bmatrix} \begin{Bmatrix} u_{n-1} \\ u_{n+1} \end{Bmatrix}$$

(6.6)

$$= \begin{Bmatrix} f_{n-1} - D_{12}(D_{11}+D_{22})^{-1}f_n \\ f_{n+2} - D_{21}(D_{11}+D_{22}I^{-1}f_n \end{Bmatrix}$$

Repeated use of this procedure will double the number of layers each time, but $(D_{11}+D_{22})$ must be well conditioned in any step. This corresponds to demanding that ω is not an eigenfrequency for a cylinder of the actual length which is clamped at the ends. If damping is included, all the eigenfrequencies become complex, and as the driving frequency ω is always real, it cannot be an eigenfrequency.

The primary cost enters in the inversion of $(D_{11}+D_{22})$. The cost of inverting a band-structured matrix of size, N and band width B is αNB^2 where α is a constant. A super element of 2^m layers with M degrees of freedom would have $(2^m-1)M$ internal degrees of freedom and a band width of M. Consequently direct condensation would cost about $\alpha(2^m-1)M^3$. Consecutive doubling would have to be done m times and cost about αmM^3 plus some matrix multiplications.

If a transducer is supplied with a backing, the backing will generally be much larger than the piezoelectric element. To include the backing in the analysis would then seriously increase the computational cost, but as it fortunately does not need to be very accurately represented it is generally sufficient to assume it to be cylindrical and then make a super element for it. As the backing also is highly damping the boundary condition on the far end is not very important and the nodes at that end may also be eliminated and thus provide a "backing element" which in use resembles that of the fluid half-space.

6.2. Infinite waveguides

The modes of propagating waves on an infinite waveguide may also be analysed by considering it as an infinite sequence of identical layers. The only possible modes are those which can propagate from one layer to the next without changes other than a phase shift. The displacements are then given by

$$u_n = e^{-i\beta n} u_o \qquad (6.7)$$

where ß is a propagation constant, which is the product of the wavenumber, k and the layer thickness, t. The equation of motion is

$$D_{21}u_{n-1} + (D_{11} + D_{22})u_n + D_{12}u_{n+1} = 0 \tag{6.8}$$

where D_{11} through D_{22} form the stiffness matrix for a single layer. (6.7) is substituted into (6.8), and when the stiffness matrix for a single layer can be split up in a stiffness and a mass matrix an eigenvalue problem of the following form is obtained.

$$\{(e^{i\beta}K_{21} + (K_{11} + K_{22}) + e^{-i\beta}K_{12}) - \omega^2(e^{i\beta}M_{21} + (M_{11} + M_{22}) + e^{-i\beta}M_{12})\}\, u_o = 0 \tag{6.9}$$

In a lossless waveguide the wave must propagate either without attenuation and ß set as real, or the wave must be standing and ß purely imaginary. If ß is real (6.9) is a Hermitian eigenvalue problem because $(K_{12}-K_{21})$ is antisymmetric. If ß is imaginary (6.9) become real and symmetric. Any choice of a purely real or imaginary ß would give a set of real eigenfrequencies ω_n, by solution of (6.9) for which waves can propagate with the wavenumber $k = \beta/t$. The shapes of the "propagating modes" are given by the eigenvectors.

The relation between k and ω_n is called the frequency relation or the dispersion relation. It can be used to determine both the phase velocity

$$c_\phi^n = \frac{\omega_n}{k} \tag{6.10}$$

and group velocity

$$c_g^n = \frac{\partial \omega_n}{\partial k} \tag{6.11}$$

Analysis of waveguides can also be carried out by incorporating the wave nature in the axial direction - similar to (6.7) - [56]. The elements will then be of one dimension less, but will have the same number of degrees of freedom per node. It leads to an eigenvalue problem of equal size as (6.9). If the thickness of the layer is chosen to be a little smaller than the lateral dimensions of the elements the accuracies of the two methods should be almost equal.

Analysis of waveguides as an infinite sequence of layers has another important aspect. It may be used to investigate the element model and various characteristics of it. Comparison of the finite element method and the finite difference method for one-dimensional wave propagation can be investigated [57, p. 33]. Spurious reflections due to element size differences can also be investigated by a very similar method [58]. In Section 8.4 the method is used to determine an optimal mixture of consistent and lumped mass in a way which resembles that of [57]. The analysis in [57] is not restricted to waveguides, but is also applied to plane problems.

7. COMPUTER PROGRAMS

To examine the ability of the finite element method to model piezoelectric ultrasonic transducers, two computer programs were written. The first program performs a forced-response analysis for single frequencies, the other makes an eigenfrequency analysis. They are both written in FORTRAN and the major parts of the two programs are identical. They employ the piezoelectric elements which are described in Section 4. The element matrices are

assembled into a global stiffness- and a global mass-matrix. The global matrices are then used to set up a system of equations or a standard eigenvalue problem, where the boundary conditions are taken into account. Prescribed degrees of freedom are eliminated.

7.1. Forced response analysis

The program for forced response analysis can take hysteretic damping into account by accepting complex elastic constants. It can utilize the super elements, which are described in Section 6. Radiation losses into a fluid half-space may also be included. The system of equations, which is set up has a coefficient matrix, which is complex and symmetric. The system is solved by subroutines from the LINPACK subroutine package [59]. These subroutines utilize the band structure of the equations but not the symmetry. The boundary conditions are prescribed displacements or forces and electric potential or electric charge in any combination at any node. The results are presented by plots of axial and radial displacements. The displacements are also visualized by a plot of the deformed element grid. These plots show instantaneous values of the nodal variables for any preselected phase angle. They always show half a cross section of the body. In the half-space the pressure on the axis and in the far-field also may be shown in different mappings.

7.2. Eigenfrequency analysis

The other computer program is almost identical to the first, except that the subroutines for solving a system of linear equations have been replaced by subroutines for solving the standard eigenvalue problem [60]. These subroutines are written to solve real symmetric eigenvalue problems. Complex eigenvalue problems can be decomposed into twice as large real eigenvalue problems. Hermitia problems become symmetric by this decomposition whereas complex symmetric problems become unsymmetric. It is therefore not immediately possible to include either internal damping or radiation losses. Even if it had been straightforward,

the cost of solving twice as large a eigenvalue problem is considerable. The real part of the eigenfrequencies is practically unaffected by the damping, and the effect on the eigenvector is primarily a phase shift due to the net energy flow.

The subroutines for solving the problem are based on a method which is called inverse subspace interation [38]. A group of eigenvectors are iterated simultaneously, and the eigenvectors with eigenvalues closest to zero are found. A frequency shift may be used to increase the convergence rate and to select a frequency range of interest. If two or more eigenfrequencies were almost identical problems with the convergence rate were experienced. These were overcome by introducing a two-step procedure. First the total group of eigenvectors was iterated 25 to 100 times. Then subgroups with almost identical eigenfrequencies are identified. A frequency shift to just below the subgroup was performed and the subgroup was iterated with a greatly increased convergence rate as a result. Both steps could be repeated as many times as desired. A typical example could be to iterate on 15 eigenvectors to get 10 which had converged. Whereas 200 iterations on the total group did not provide 10 converged eigenvectors, 25 iterations on the total group followed by 50 on subgroups did provide 10 converged eigenvectors.

8. EXAMPLES

The programs have been tested against a number of simple solutions to check that they have been correctly programmed. In the case of uniaxial stress and other solutions with linear displacement fields the forced response analysis program reproduced the results exactly as expected. This program was also used to calculate the displacements in a circular disk, supported at the edge and loaded by a static pressure on one face. The ratio of the radius to the thickness of the disk was 30. The finite element model was built up of element pairs, which together formed

a rectangular ring. The test was performed with different element grids. As the stresses are constant in the thickness direction within each element at least two element pairs in the thickness direction are necessary to model the plate; to obtain any appreciable accuracy more elements must be used.

Furthermore it was found that the length of the sides of the element pairs should not differ too much (1:3). If the plate is modelled with 180 × 4 element pairs the deflection of the center was found within 4.5%, when compared with the solution in [61, p. 109]. This result is acceptable when the number of elements in the thickness direction is considered, but it also indicates that second-order elements are desirable to include. The dynamic properties were tested against vibrations of infinite layers and thin rods. The infinite layer is also used in Section 8.4.

8.1. Eigenfrequencies of a piezoelectric disk

The first example of technical interest is to determine the modes in a freely vibrating, fully electroded, piezoelectric disk. The calculated eigenfrequencies are compared with measurements. A disk of PZ-29 (Ferroperm) with radius a = 6.3 mm and thickness 2 h = 1.28 mm was used as an example. PZ-29 is very similar to PZT-5H (Vernitron), and as the available material data for PZ-29 were insufficient those for PZT-5H were used in the calculations (see Appendix A). As only modes which can be excited electrically are of interest, it is sufficient to consider half of the disk by utilizing the symmetry. To determine the size of the elements needed to model the disk, a forced response analysis of the disk near the thickness eigenfrequency was performed for different element sizes. It was decided to model half of the disk with 30 × 5 element pairs. At the thickness eigenfrequency this gives about 20 elements per wavelength in the thickness direction and slightly less in the radial direction.

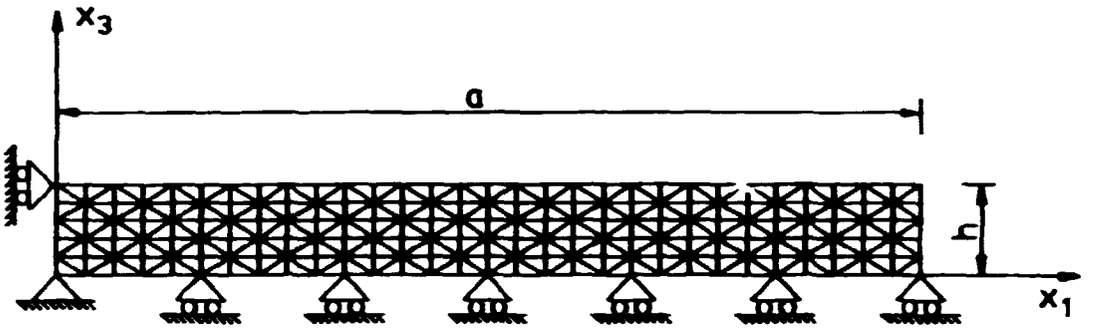

Fig. 8.1. Finite element model of half of a freely vibrating disk.

The first sixteen modes found by the eigenfrequency analysis program are shown below.

The first five modes may be identified as radial modes where the electric field and the displacements approximately are given as products of trigonometric functions in the axial direction and Bessel functions in the radial direction. Mode number six through eight also resembles radial modes, but near the edge the displacements are too large and irregular. Modes nine through eleven have almost equal eigenfrequencies. This slowed down the convergence of eigenvalue analysis so much that the frequency shift had to be utilized to obtain convergence. The eigenfunctions seem quite complicated and they have not been classified presently. They have large shear strains. They are expected to be very sensitive to any change in geometry or material data. Mode twelve is regular and has also large shear strains. The remaining four of the modes shown have not been classfied either, but mode 14 has an eigenfrequency very close to the simple thickness eigenfrequency, although it can hardly be characterized as that.

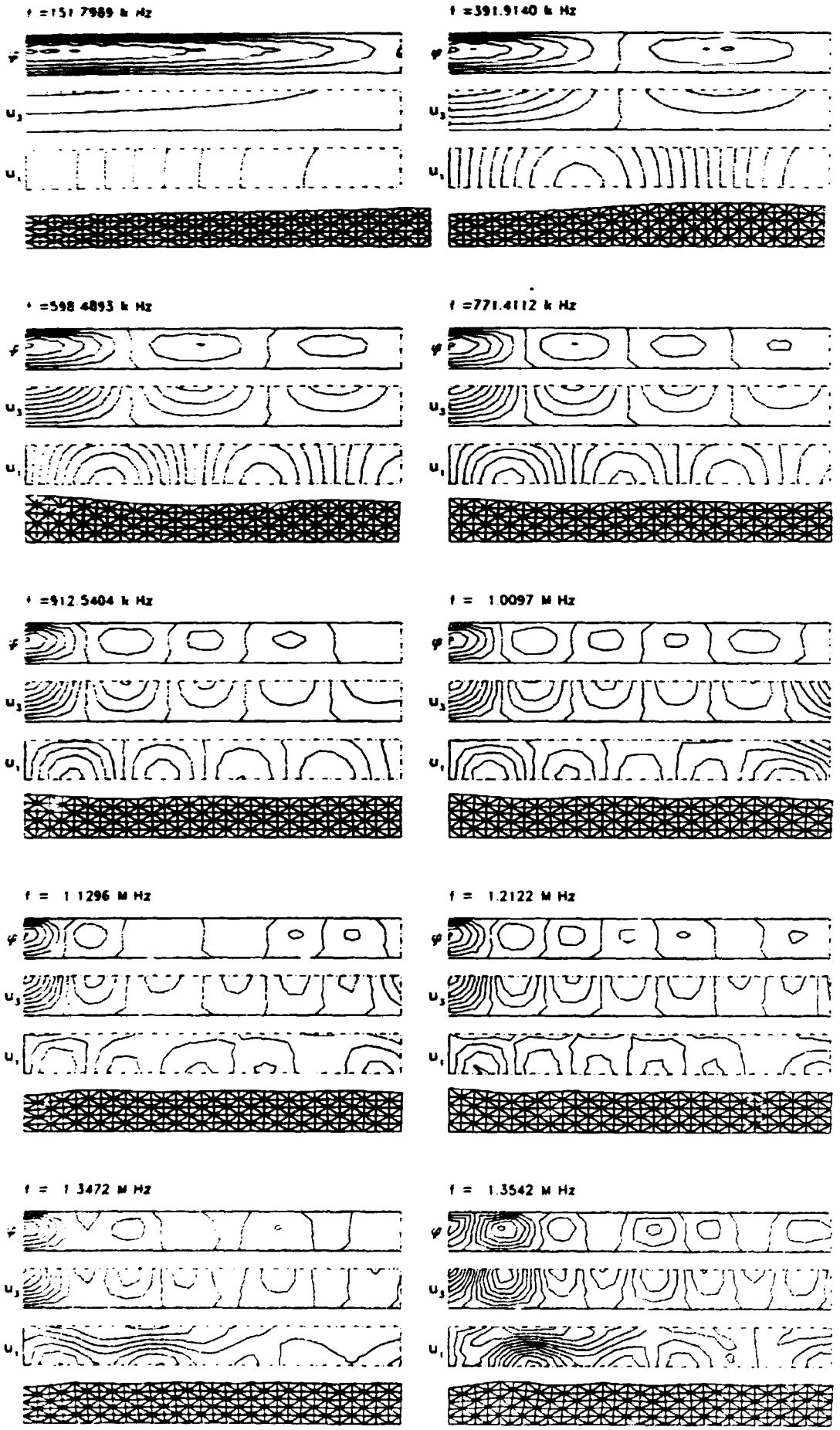
f =151.7989 k Hz
f =391.9140 k Hz
f =598.4893 k Hz
f =771.4112 k Hz
f =912.5404 k Hz
f = 1.0097 M Hz
f = 1.1296 M Hz
f = 1.2122 M Hz
f = 1.3472 M Hz
f = 1.3542 M Hz

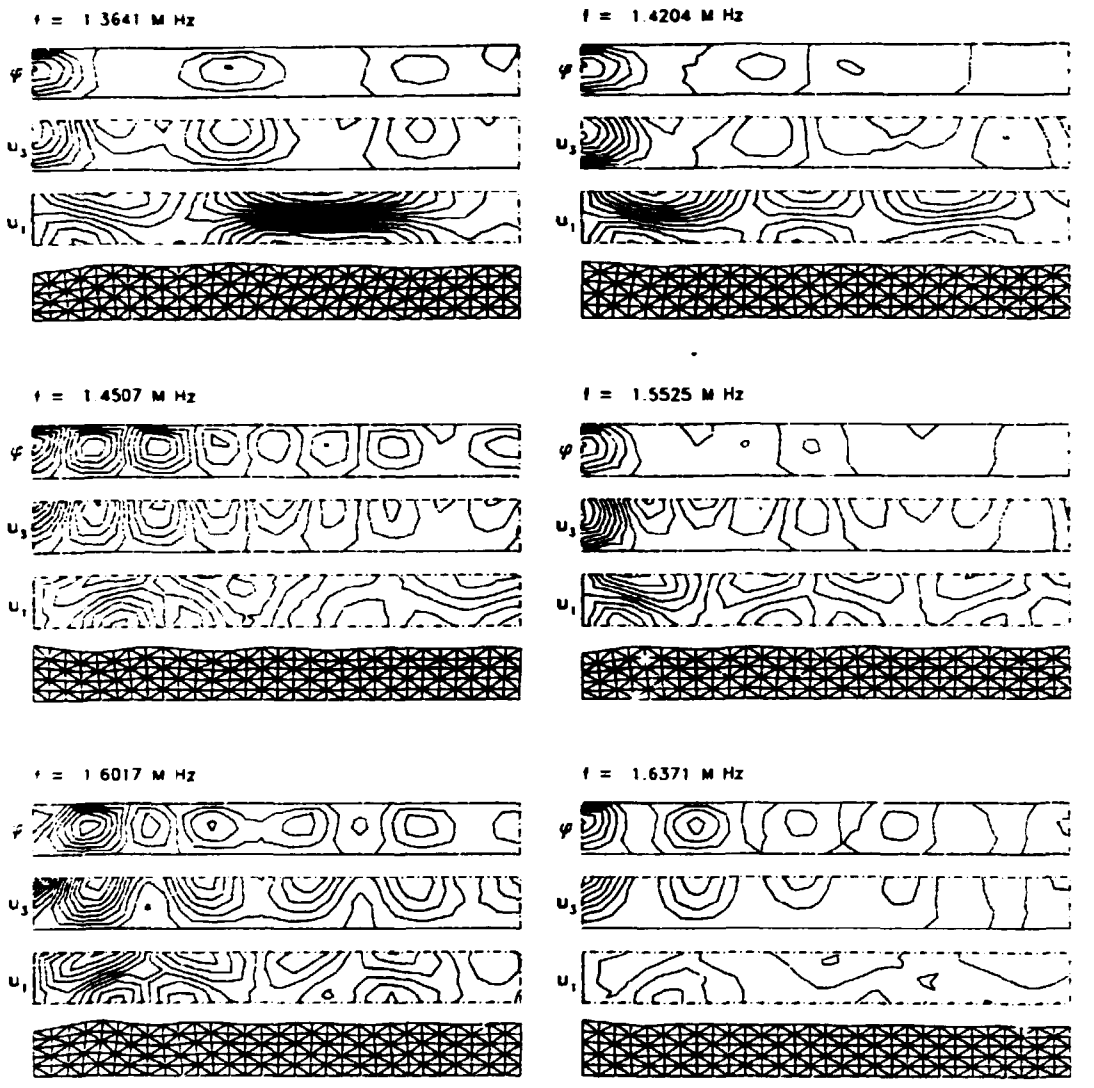

Fig. 8.2. Contour plots of the electric potential and the displacements for the first sixteen modes of a freely vibrating piezoelectric ceramic disk.

The calculated eigenfrequencies were compared with eigenfrequencies determined from electrical admittance measurements. The disk was prepared and the measurements carried out at Brüel & Kjær. The results are shown in the table below:

None of the calculated eigenfrequencies differ with more than 3.5% from the measured ones. Typically the difference is about

2%. This result is very satisfying when the inaccuracy of the material data is considered. Furthermore, it can be noticed that especially the first radial modes systematically have to low eigenfrequencies. A minor adjustment of the material data, could possibly provide a better match for these eigenfrequencies.

Table 8.1. Comparison of measured and calculated eigenfrequencies for a piezoelectric disk a = 6.3 mm. 2 h = 1.3 mm.

Measured [M Hz]	Calculated [M Hz]	Difference [%]
0.157	0.152	-3.2
0.403	0.391	-3.0
0.616	0.598	-2.9
0.790	0.771	-2.4
0.921	0.913	-0.9
1.001	1.010	0.9
1.148	1.130	-1.6
1.256	1.212	-3.5
1.334	1.347	1.0
-	1.354	(-1.0)
1.368	1.364	-0.3
1.434	1.420	-1.0
1.478	1.451	-1.9
1.549	1.553	0.3
1.604	1.602	-0.1
	1.637	

8.2. Electrical admittance of a loaded ultrasonic tranducer

The next test was to make a simple transducer with the previously used piezoelectric disk. The disk was mounted in a plexiglass house, and had a backing attached to it.

The backing was composed of equal volumes of epoxy and a filler with a seven times higher mass density. The filler consists of grains which are not uniformly distributed in the epoxy matrix. In any event, the backing was modelled as if it were homogenous. The material data was estimated on the basis of measurements of mass density, sound velocity and attenuation (see Section 4.3).

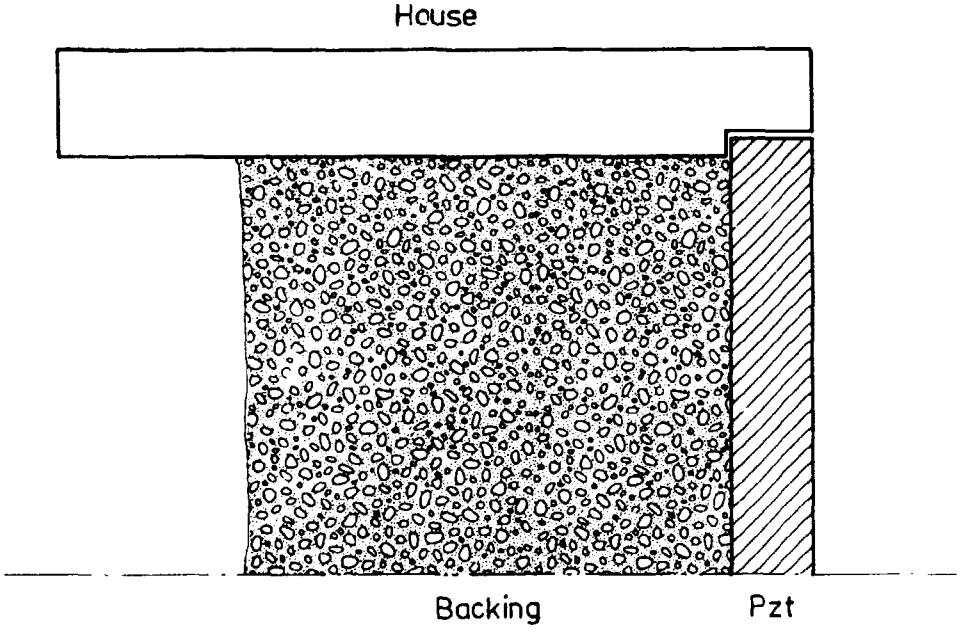

Fig. 8.3. Simple test transducer.

Poisson's ratio was assumed to be 0.35 and the attenuation of shear waves was slightly rounded up.

The piezoelectric disk was modelled by 32 × 8 element pairs. The backing was composed of two layers by which the element size was increased, and a super element of 32 layers with eight elements in each.

The plexiglass house has been omitted from the analysis. The normal displacements are represented by a polynomial of degree 30, where only even powers in x, are present, i.e. the polynomial expansion (5.11) has been truncated to 15 terms. It was controlled that this truncation was sufficient by comparing it with results

for 25 terms at a single frequency; no appreciable difference was found.

The electrical admittance of the transducer has been calculated in steps of 0.05 MHz. in the range 0 to 2 MHz. A comparison with the measured admittance is shown below. All measurements and preparations have been made at Brüel & Kjær.

The calculated admittance is about 1.5 times larger than the measured. Apart form this mis-scaling the curves show good qualitative agreement.

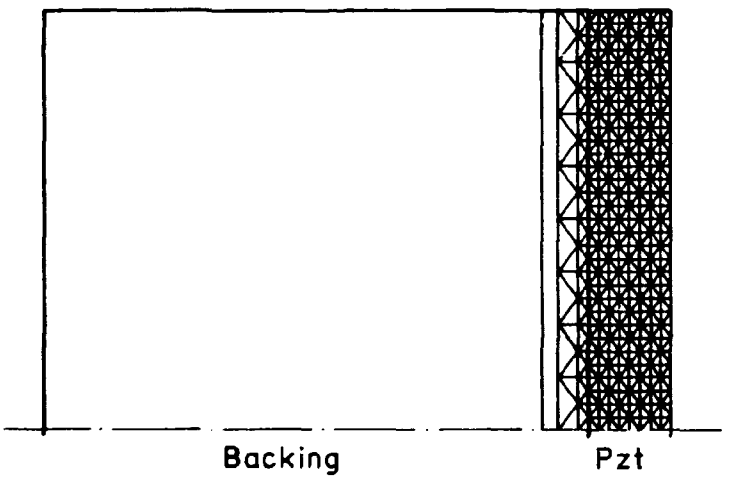

Fig. 8.4. Finite element model of the transducer in Fig. 8.3.

The course for the mis-scaling has not been identified but several possibilities exists. The housing has not been modelled. The transducer is not baffled and the material data are relatively inaccurate. A mis-scaling of about the same size of the admittance curve can be seen in [24]; also Cowdry and Willis [39] conclude that their finite element approach needs refinements, before they can give the admittance curve.

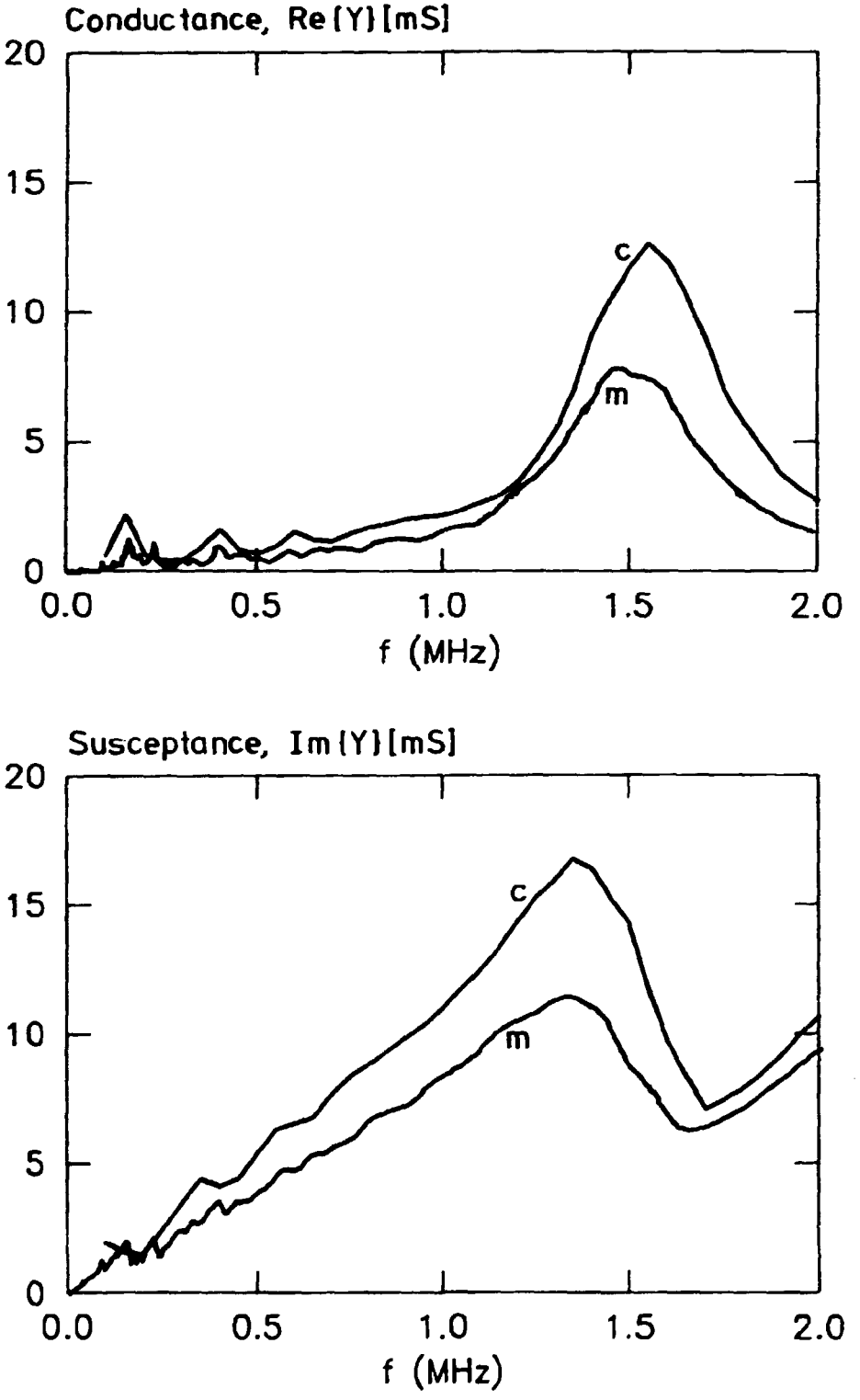

Fig. 8.5. A comparison between calculated (c) and measured (m) admittance of the test transducer shown as conductance and susceptance on different graphs.

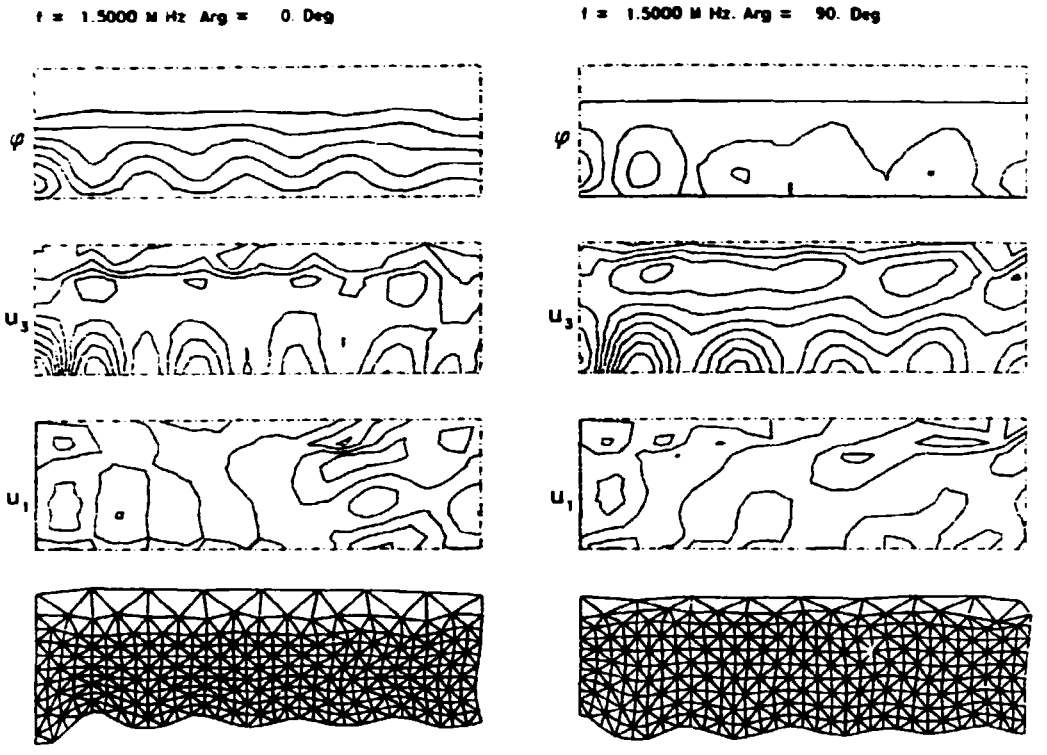

Fig. 8.6. The vibrations of the loaded transducer at the frequency of maximum admittance (c.f. Fig. 8.5).

The calculated vibrations for the transducer at the frequency of maximum admittance is shown in Fig. 8.6.

8.3. Far-field measurements

The most direct way to verify the finite element calculations would be, of course, to measure the displacement amplitudes directly, but this has not been attempted due to the small amplitudes ($\sim 10^{-8}$m). The radiated field is in itself interesting and provides also a good test of the calculations. For an unfocused transducer the far-field is equivalent to the two-dimensional Fourier transform of the normal velocity, and far-field measure-

ments therefore is the simplest possible check of the velocity distribution.

The measurements were carried out with an existing equipment for characterization of three-dimensional sound fields [62]. This equipment uses the pulse-echo method, and is primarily intended for characterization of focused transducers. It was attempted to measure both the near-field on the axis and the far-field as both can be expressed explicitly by the normal velocity (cf. Section 5).

The near-field measurements were given up because the primary pulse lasted for about 10 μs and hence made the taking of measurements closer than 8 mm to the transducer impossible. At greater distances the field on the axis primarily reflects the average velocity, v_o.

Six different transducers were built at the Laboratory of Industrial Acoustics at the Technical University of Denmark. All of them had their sound field measured. For measurements of the far-field the equipment has a limitation which makes it possible to measure the farfield in only 20 different distances from the axis. As the equipment uses ultrasonic pulses and not continuous waves, and the signal-to-noise ratio is limited to about 30 dB it was decided not to attempt to remove the limitation on the number of different distances. For the same reason only the measurements of the simplest transducer is presented. The transducer is shown on Fig. 8.7.

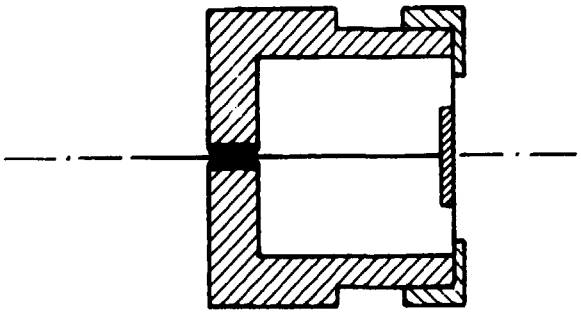

Fig. 8.7. Transducer (# 1) for sound field measurements.

The transducer consists of an air-filled brass house, where the front is covered by a 6 μm thick polyester film to which the piezoelectric disk is attached. The sound field at 74 mm from the front of the transducer is shown in Fig. 8.8.

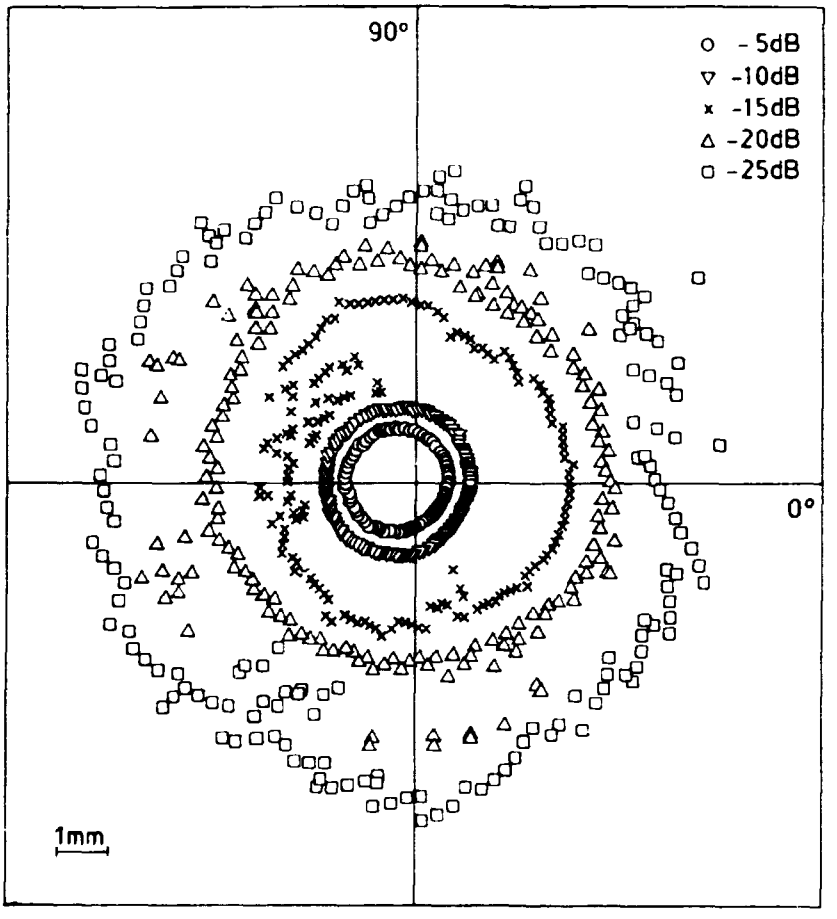

Fig. 8.8. Points of equal sound intensity 74 mm from the transducer shown in Fig. 8.7.

The sound field can be seen to be almost axisymmetric, but also to be slightly eccentric. In Fig. 8.9 the intensity is shown along four different lines all of which passes close to the center of the sound field.

The first side lobe is 13 - 15 dB below the main lobe. If the ceramic disk had a uniform velocity distribution and were harmonically excited, the side lobe would have been 17.6 dB below the main lobe. When the excitation contains more than a single

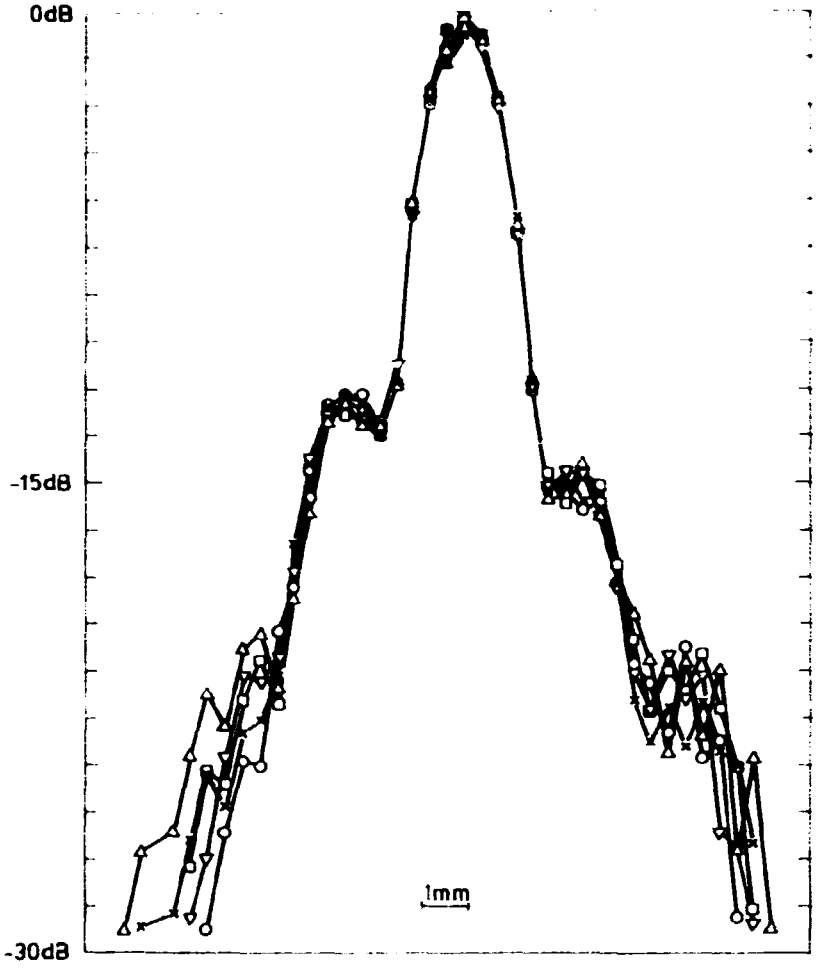

Fig. 8.9. Radiation pattern of test transducer.

frequency the first side lobe should be less pronounced, as every frequency component contributes to both the main lobe and all the side lobes; but the direction of the main lobe is fixed, whereas the directions of the side lobes are frequency dependent. Hence, it may be concluded that the velocity distribution of the transducer is far from uniform.

8.4. Simple thickness vibrations

The exact solution for simple thickness vibrations of an infinite plate is given in Section 3.1. It has a frequency equation which

is easily solved numerically (3.7). The simple thickness vibrations of an infinite plate can also be investigated by a finite element model. The model may consist of a cylinder, as shown on Fig. 8.10, where zero radial motion has been imposed on every node. The symmetry is utilized and only half of the thickness is modelled.

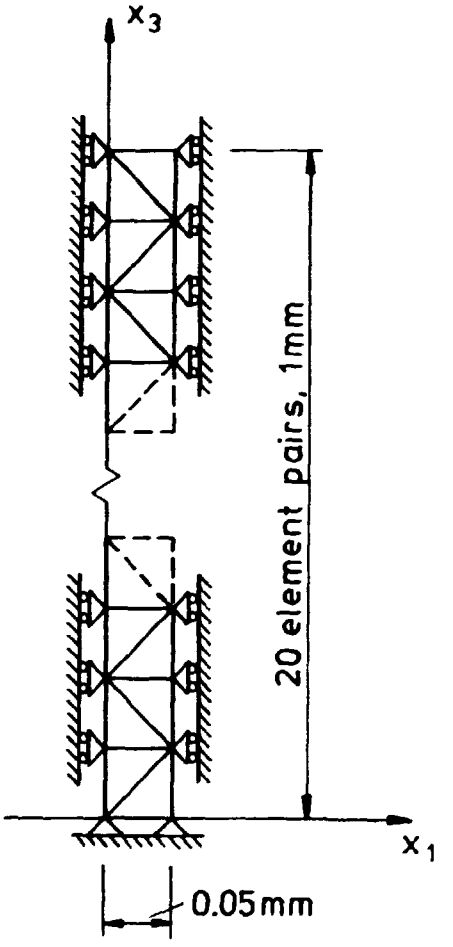

Fig. 8.10. Finite element model for investigating of simple thickness vibrations of an infinite plate.

The finite elements are arranged in pairs, each of which forms a ring with quadratic cross section. The side length is ℓ. The first ten simple thickness eigenfrequencies of an infinite plate

were found by solution of (3.7) and compared with those found by eigenfrequency analysis on the finite element model. This also gives an indication of how the solution degrades, when the element size becomes comparable with the wave-length. The result is shown in Table. 8.2. The propagation constant $\beta = k\ell = 2\pi\ell/\lambda$ gives the phase shift over a single element pair.

Table 8.2. Comparison of non-dimensionalized eigenfrequencies for an infinite plate of PZT-5H found from the frequency equation (3.11) (hk) and found from a finite element model with 20 layers (hk').

n	hk	hk'	difference [%]	β
1	1.383	1.383	0.0	0.07
2	4.656	4.663	0.2	0.23
3	7.820	7.854	0.4	0.39
4	10.971	11.066	0.9	0.55
5	14.119	14.322	1.4	0.71
6	17.264	17.636	2.2	0.86
7	20.407	21.025	3.0	1.02
8	23.551	24.500	4.0	1.18
9	26.694	28.070	5.2	1.33
10	29.836	31.732	9.7	1.49

It can be observed that the eigenfrequencies found by the finite element method are too high, i.e. the kinetic energy at a given frequency is too low compared with the elastic energy. The opposite, and stronger effect can be seen, if the mass matrix is lumped, in which case it has only non-zero elements in the diagonal. The phenomenon can be explained by a one-dimensional model [57].

Consider an infinite rod with cross-sectional area A, Young's modulus E, and mass density ρ. The dynamic stiffness matrix D for a piece of the rod of length ℓ is

$$D = \frac{EA}{\ell}\begin{Bmatrix} 1 & -1 \\ -1 & 1 \end{Bmatrix} - \omega^2\rho A\ell\left(\begin{Bmatrix} 1/2 & 0 \\ 0 & 1/2 \end{Bmatrix} - \alpha\begin{Bmatrix} 1/6 & -1/6 \\ -1/6 & 1/6 \end{Bmatrix}\right) \tag{8.1}$$

where $\alpha = 1$ corresponds to a consistent mass matrix and $\alpha = 0$ to a lumped one. This matrix can be used in the analysis of infinite waveguides from Section 6.2. Inserted in (6.9) it gives

$$\omega\ell = \sqrt{\frac{E}{\rho}}\sqrt{\frac{6(1-\cos\beta)}{3-\alpha(1-\cos\beta)}} \tag{8.2}$$

β is the propagation constant $k\ell$. Due to the discretization the wave has become dispersive, as the phase velocity is $c_\phi = \omega\ell/\beta$. The phase velocity normalized with the nominal velocity $c_0 = (E/\rho)^{1/2}$ is shown in Fig. 8.11.

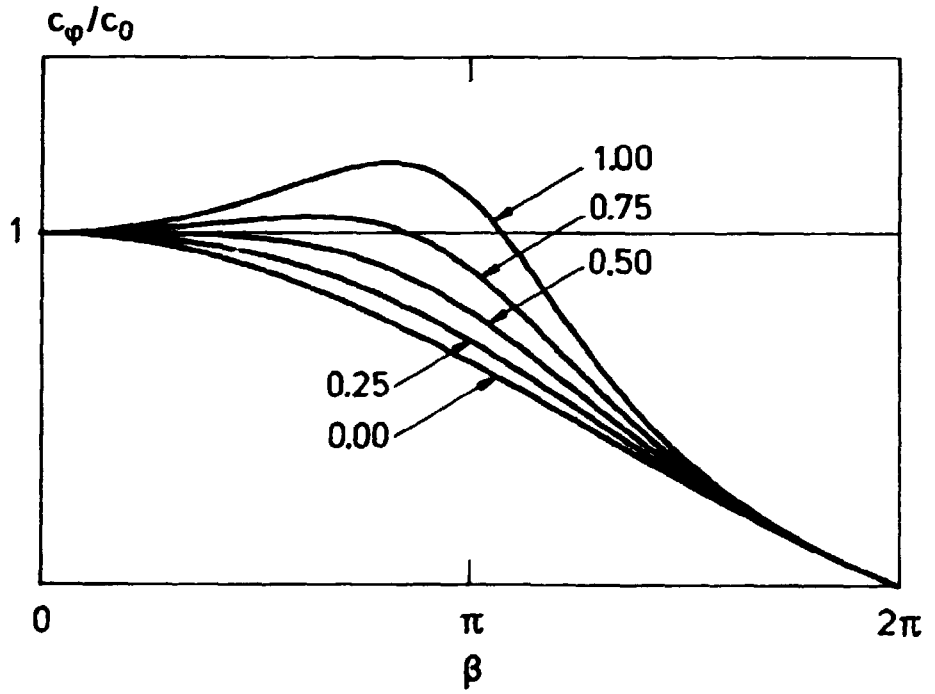

Fig. 8.11. The phase velocity in a one-dimensional linear waveguide model as a function of the propagation constant $\beta = k\ell$ for different values of α.

It can be seen that neither a consistent nor lumped mass matrix gives the best fit to the nominal velocity. For low frequency $\alpha = 0.5$ is the optimum [57, p. 33]. For specific problems it may be better to choose larger values of α. If the velocity is allowed to vary within $(1-\varepsilon) < c_\phi/c_o < (1+\varepsilon)$ the optimum values of α and the maximum values of β are given in the table below.

Table 8.3. Optimal values of α, and maximum values of β for given acceptable errors on the phase velocity due to discretization. Estimated by a one-dimensional model.

ε [%]	α_{opt}	β_{max}
0.1	0.535	1.27
0.2	0.555	1.54
0.5	0.580	1.84
1.0	0.613	2.14
2.0	0.663	2.49
5.0	0.795	3.07

To verify this, the eigenfrequencies of the infinite layer were calculated with $\alpha = 2/3, 1/2, 0$. They were then compared with those previously calculated for $\alpha = 1$ and the axact solution. The relative errors are shown below.

The savings obtained using this method are considerable. If the element size may be increased by a factor $a > 1$ in both directions the number of nodes is reduced with a factor a^{-2}. The cost of solving the system of equations is then reduced by a factor of about a^{-6}.

Table 8.4. Error on estimated eigenfrequencies in percent for an infinite plate with α = 0, 1/2, 2/3, 1.

n \ α	0	1/2	2/3	1.00
1	-0.0	-0.0	+0.0	0.0
2	-0.3	-0.1	-0.0	0.2
3	-0.9	-0.2	-0.0	0.4
4	-1.7	-0.4	-0.0	0.9
5	-2.8	-0.7	-0.03	1.4
6	-4.2	-1.2	-0.1	2.2
7	-6.1	-1.8	-0.3	3.0
8	-	-2.6	-0.5	4.0
9	-	-4.3	-1.1	5.2
10	-	-	3.4	7.7

9. CONCLUSIONS

Analyses of piezoelectric ultrasonic transducers can be carried out by different methods. The dominant method used today is the equivalent circuit (or similar one-dimensional methods). This method gives a simple and still quite accurate representation of the transducer. This method is practical to use especially, in connection with analysis of the electrical circuit. It can be applied to structures of complex shape and they may be damped. The main disadvantage of the method is that the parameter values in the model must be found by other means. The parameter values are often found by introducing greatly simplifying assumptions - which of course influences their accuracy - but they can also be determined from measurements or analyses by other methods.

Simple structures can be analysed by the Rayleigh-Ritz method or - in the case of plates - plate theory. Both methods may provide detailed and accurate solutions, but they are difficult to apply

to structures of complex shape consisting of different materials. Damping may also be a problem to handle by these methods.

The finite element method is applicable to complex structures which consist of different materials. Piezoelectricity as well as internal damping is easily included in the elements. Radiation damping may also be included via integral representations. The necessary number of elements to model a structure depends on the complexity of the structure and the frequency of the excitation. Elements with linear variations in the displacements and the electric potential must be small compared with any geometric length scale as well as any wavelength involved in the problem. For ultrasonic transducers the wave length generally determines the element size and even guite simple transducers may demand a large number of elements. To fully include the piezoelectric effect demands an electrical degree of freedom in each node. For these reasons the computational cost may also be high.

Due to the great applicability of the finite element method, it was decided to investigate it further, by developing two computer programs based on the method. To keep the computational cost low, the programs were restricted to axisymmetric structures. For practical reasons, only the triangular ring element with linear variations of displacements and electric potential has been implemented. This element is unrestricted in orientation and location, and it involves no numerical integration. Internal damping is included in the form of hysteretic damping by allowing complex elastic constants.

Radiation damping has been included by assuming that the transducer is baffled and radiates into a fluid half-space. The velocity potential in the half-space is given by an integral representation from which the reaction force on the transducer is found. Both the normal velocity and the pressure on the surface of the transducer are expanded in orthogonal polynomials. The relation between the expansion coefficients is given by the generalized impedance matrix. The stiffness matrix of the half-space - in the finite element-sense - is easily found from the generalized impedance matrix. The effort needed to calculate the

half-space stiffness matrix is negligible, in comparison with that of solving the finite element equation. The expansion of the normal velocity can also be used to express the sound field in the half-space. On the axis and in the far-field the sound field can be explicitly expressed by the expansion coefficients.

If the structure is cylindrical, a finite element model of it may consist of a series of equal layers, in which case a special stacking procedure can be used to obtain a computational saving, which is similar to that obtained by the "fast Fourier algorithm". This has been utilized to model the backing of the transducer, which is a damping material attached to the back of the piezoelectric element.

Comparison with measurements and exact solutions has shown that the finite element method can be used to analyse ultrasonic transducers. Eigenfrequencies can be determined accurately. The main characteristics of the electrical impedance can also be recovered, but the numerical value has been experienced to be as much as 50% wrong with a reasonable element grid. The accuracy of the displacements has not been determined for any non-trivial cases, but it must be expected to be much less than that of the eigenfrequencies, and to be much dependent on the element size.

The computer programs were primarily developed to investigate the finite element method for the purpose of analyzing of ultrasonic transducers. It must be concluded that the method is useful because of the ease by which it can handle structures of elastic as well as piezoelectric materials, damping, and different boundary conditions. Among the disadvantages of the method is that it only gives the influence of various parameters indirectly, and that it, in its present formulation can be used only in the frequency domain, whereas many applications of ultrasound make use of pulses.

Much can be done to reduce the computational cost. The most straightforward possibility is to implement a second-order finite element [63]. Extended use of super elements is another possibility. The fact that quite simple methods work well also

suggests that it may be advantageous to separate out the dominant undamped purely elastic problem, and solve it first. Damping and piezoelectric coupling may then be included as a pertubation to that problem. This has been shown to work well at least for the piezoelectric coupling [44]. The regularity of the first modes of a circular disk and their resemblence to radial modes suggests that for that case it should be possible to find a small set of test functions to be used with the Rayleigh-Ritz method, and provide good results. The developed computer program may be useful to find the test functions.

REFERENCES

[1] HUETER, T.F. and BOLT, R.H. (1955). Sonics (Wiley, New York) 80 p.

[2] FRIDERICK, J.R. (1965). Ultrasonic Engineering (Wiley, New York) 379 p.

[3] HUNT, J.W., ARDITI, M. and FOSTER, F.S. (1983). Ultrasound Transducers for Pulse-Echo Medical Imaging. IEEE Trans. Biomed. Eng. BME-30, 453-481.

[4] CADY, W.G. (1964). Piezoelectricity New rev. ed. (Dover, New York) Vol. 1-2.

[5] MASON, W.P. (1948). Electromechanical Transducers and Wave Filters, 2. ed. (van Nostrand, Priceton) 419 p.

[6] LEEDOM, D.A., KRIMHOLTZ, R. and MATTHAEI, G.L. (1971). Equivalent circuits for transducers having arbitrary even- or Odd-symmetry piezoelectric excitation, IEEE Trans. Sonics Ultrason. SU-18, 128-141.

[7] MINDLIN, R.D. (1955). An Introduction to the Mathematical Theory of Vibrations of Elastic Plates. U.S. Army Signal Corps, Contract DA-36-039, SC-56772.

[8] GAZIS, D.C. and MINDLIN, R.D. (1960). Extensional Vibrations and Waves in a Circular Disk and a Semi-Infinite Plate. J. Appl. Mech. 27, 541-547.

[9] HOLLAND, R. AND EER NISSE, E.P. (1967). Variational Evaluation of Admittances of Multielectroded Three-Dimensional Piezoelectric Structures. IEEE Trans. Sonics Ultrason., SU-15, 119-132.

[10] TIERSTEN, H.F. (1969). Linear Piezoelectric Plate Vibrations. New ed. (Plenum, New York). 212 p.

[11] SLATER, J.C. (1959). Microwave Transmission. (Dover, New York). 309 p.

[12] MORSE, P.M. and INGARD, K.U. (1968). Theoretical Acoustics, (McGraw-Hill, New York) 927 p.

[13] RAYLEIGH., J.W.S. (1894)(1945). The Theory of Sound (Dover, New York) Vol. 1-2.

[14] KING, L.V. (1934). On the radiation field of the Piezo-Electric Oscillator and the Effect of Viscosity on Transmission, Can. J. Res. Sect. A. 11, 135-155.

[15] O'NEIL, H.T. (1949). Theory of Focusing Radiators. J. Acoust. Soc. Am. 21, 516-526.

[16] DEKKER, D.L., PIZIALI, R.L. and DONG, E. (1974). Effects of Boundary Conditions on the Ultrasonic-Beam Characteristics of Circular Disks. J. Acoust. Soc. Am. 56, 87-93.

[17] GREENSPAN, M. (1979). Piston Radiator: Some Extensions of the Theory. J. Acoust. Soc. Am. 65, 608-621.

[18] KRENK, S. (1983). Geometrical aspects of acoustic radiation from a shallow spherical cap. J. Acoust. Soc. Am. 74, 1617-1622.

[19] ALLIK, H. and HUGHES, T.J.R. (1970). Finite Element method for Piezoelectric Vibration, Int. J. Num. Meth. Eng. 2, 151-157.

[20] HUNT, J.T. KNITTEL, M.R. and BARACH, D. (1973). Finite element approach to acoustic radiation from elastic structures J. Acoust. Soc. Am., 55, 269-280.

[21] ALLIK, H., WEBMAN, K.M. and HUNT, J.T. (1974). Vibrational response of sonar transducers using piezoelectric finite elements. J. Acoust. Soc. Am., 56, 1782-1791.

[22] KAGAWA, Y. and YAMABUCHI, T. (1979). Finite Element Simulation of a Composite Piezoelectric Ultrasonic Transducer IEEE Trans. Sonics Ultrason. SU-26, 81-88.

[23] DÉCARPIGNY, J-N. (1980). Application de la Méthode des Eléments Finis a l'étude de Transducteurs Piézoélectriques, (Ph.D. Thesis) (Universilé des Sciences et Techniques de Lille, Lille). W 618.

[24] NAILLON, M., CORRSANT, R.H. and BESNIER, F. (1984). Analysis of piezoelectric structures by a finite element methode Acta electron, 25, 4, 341-362.

[25] IEEE Standard on Piezoelectricity, ANSI/IEEE Std 176-1978, In: IEEE Trans. Sonics Uttrason. SU-31, No. 2, Part II (1984).

[26] BERLINCOURT, D., CURRAN, D.R. and JAFFE, H. (1964). Piezoelectric and Piezomagnetic Materials and Their Function in Transducers. Physical Acoustics, (Academic Press, New York) Vol. 1A, 167-270,

[27] LOVE, A.E.H. (1945). A Treatise on the Mathematical Theory of Elasticity 4. rev. ed. (Cambridge University Press (1927)), (Dover, New York) 644 p.

[28] MEITZLER, A.H., O'BRYAN, H.M. and TIERSTEN, H.F. (1973). Definition and Measurement of Radial Mode Coupling Factors in Piezoelectric Ceramic Materials with Large Variations in Poisson's Ratio, IEEE Trans. Sonics Ultrason, SU-20, 3, 233-239.

[29] RASMUSSEN, K. (1981). Analogier mellem mekaniske, akustiske og elektriske systemer, 2. udg. (Polyteknisk Forlag, Lyngby. 103 p.

[30] GAZIS, D.C. and MINDLIN, R.D. (1960). Extensional Vibrations and Waves in a Circular Disk and a Semi-Infinite Plate, J. Appl. Mech., 27, 541-547.

[31] TASI, J. (1971). An Asymptotic Analysis of the End Mode in a Circular Disk, J. Acoust. Soc. Am., 50, 1384-1386.

[32] IKEGAMI, S., UEDA, I. and KOBAYASHI, S. (1974). Frequency spectra of resonant vibration in disk plates of $PbTiO_3$ piezoelectric ceramics. J. Acoust. Soc. Am., 55, 339-344.

[33] SHAW, E.A.G. (1956). On the Resonant Vibrations of Thick Barium Titanate Disks, J. Acoust. Soc. Am., 28, 38-50.

[34] MINDLIN, R.D. and MEDICK, M.A. (1959). Extensional Vibrations of Elastic Plates, J. Appl. Mech., 26, 561-569.

[35] EER NISSE, E.P. (1967). Variational Method for Electroelastic Vibration Analysis, IEEE Trans. Sonics Ultrason., SU-14, 153-160.

[36] HOLLAND, R. and EER NISSE, E.P. (1968). Variational Evaluation of Admittances of Multielectroded Three-Dimensional Piezoelectric Structures, IEEE Trans. Sonics Ultrason., Su-15, 119-132.

[37] ZIENKIEWICZ, O.C. (1977). The Finite Element Method, 3. ed. (McGraw-Hill, London) 787 p.

[38] BATHE, K-J. and WILSON, E.L. (1976). Numerical Methods in Finite Element Analysis, (Prentice-Hall, Englewood Cliffs). 528 p.

[39] COWDREY, D.R. and WILLIS, J.R. (1974). Application of the finite element method to the vibrations of quartz plates. J. Acoust. Soc. Am., 56, 94-98.

[40] WINNICKI R.T. and AUYER, S.E. (1979). Geometric factors affecting hydrophone performance, J. Acoust. Soc. Am., 61, 876-81.

[41] TOMIKAWA, Y. SUGAWARA, S. and KONNO, M. (1979). Finite Element Analysis of Displacement at Base Portion of a Quartz Crystal Tuning Fork, IEEE Trans. Sonics Ultrason., SU-26, 259-261.

[42] KAGAWA, Y. and YAMABUCHI, T. (1976). Finite Element Approach for a Piezoelectric Circular Rod, IEEE Trans. Sonics Ultrason., SU-23, 379-385.

[43] KAGAWA Y. and YAMABUCHI, T. (1976). A Finite Element Approach to Electromechanical Problems with an Application to Energy-Trapped and Surface-Wave Devices, IEEE Trans. Sonics Ultrason., SU-23, 263-272.

[44] D. BOUCHER, M. LAGIER, C. MAERFELD, (1981). Computation of the Vibrational Modes for Piezoelectric Array Transducers using Mixed Finite Element-Pertubation Method, IEEE Trans. Sonics Ultrason., SU-28, 318-330.

[45] McDEARMON, G.F. (1984). The addition of piezoelectric properties to structural finite element programs by matrix manipulations, J. Acoust. Soc. Am., 76, 666-669.

[46] KRENK, S. (1984). The Triangular Elastic Ring Element with Linear Displacements, DtH-DCAMM-285)10 p.

[47] LAGASSF, P.E. (1973). Finite Element Analysis of Piezoelectric Elastic Waveguides, IEEE Trans. Sonics Ultrason., SU-20, 354-359 .

[48] FOSS, K.A. (1958). Co ordinates which Uncouple the Equations of Motion of Damped Linear Dynamic Systems. J. Appl. Mech., 25, 361-364.

[49] BELINCOURT, D. (1971). Piezoelectric Crystals and Ceramics in: Ultrasonic Transducer Materials Ed. by O.E. Mattiat, (Plenum, New York) 185 p.

[50] COLLIN, R.E. (1966). Foundations for Microwave Engineering (McGraw-Hill Kogakusha, Tokyo). 589 p.

[51] ABRAMOWITZ, M. and STEGUN, I. (1972). Handbook of Mathematical Functions (Dover, New York).

[52] ZERNIKE, F. (1934). Beugungstheorie des Schneidenverfahrens und seiner verbesserten Form, der Phasenkontrastmethode, Physica, 1, 689-704.

[53] WATSON, G.N. (1944). A Treatise on the Theory of Bessel Functions", 2. ed. (Cambridge University Press, Cambridge). 804 p.

[54] GRATSHTEYN, I.S. and RYZHIK, I.M. (1980). Table of Integrals, Series, and Products, (Academic Press, New York).

[55] GOETSCHEL, D.B., DONG, S.B., MUKI, R. (1982). A Global Local Finite Element Analysis of Axisymmetric scattering of Elastic Waves J. Appl. Mech., 49, 816-820.

[56] LAGASSE, P.E. (1973). Finite Element Analysis of Piezoelectric Elastic Waveguides, IEEE Trans. Sonics Ultrason, SU-20, 354-359.

[57] VICHNEVETSKY, R. and BOWLES, J.B. (1982). Fourier Analysis of Numerical Approximation of Hyperbolic Equations, (Siam, Philadelphia).

[58] BAŽANT, Z.P. (1978). Spurias Reflection of Elastic Waves in Nonuniform Finite Element Grids, Comp. Meth. Appl. Mech. Eng., 16, 91-100.

[59] DONGARRA, J.J., MOLER, C.B., BUNCH, J.R. and STEWART, G.W. (1979). LINPACK users' guide. (Society for Industrial and Applied Mathematics, Philadelphia).

[60] GRUBER, R. (1975). Hymnia - Band Matrix Package for Solving Eigenvalue Problems, Computer Physics Comm., 10, 30-41.

[61] BROBERG, B. [et al.] (1978). Formelsamling i hållfasthetslära. (Kungl. Tekniska Högskolan, Stockholm) (Publikation/ Institutionen för Hållfasthetslära, Kungl. Tekn. Högsk., 104) 379 s.

[62] GUNDTOFT, H.E. and NIELSEN, T. (1982). Accurate Three-Dimensional Characterization of Ultrasonic Sound Fields 8By Computer Controlled Rotational Scanning), Materials Evaluation, 40, 78-83.

[63] DUROCHER, L.L., GASPER, A., RHOADES, G. (1978). A Numerical Comparison of Axisymmetric Finite Elements, Int. J. Num. Meth. Eng., 12, 1415-1427.

[64] KRENK, S., SCHMIDT, H. (1982). Elastic Wave Scattering by a Circular Crack" Phil. Trans. R. Soc. Lond., 308, 167-198.

RESUMÉ

Analyse af piezoelektriske ultralydtransducere indebærer løsning af randværdi problemer for legemer, der er piezoelektriske, og som i almindelighed ikke kan betragtes som tabsfrie. Problemet er dynamisk ved frekvenser, hvor en typisk bølgelængde er sammenlignelig med legemets dimensioner. Legemet består af forskellige materialer, og dets udstråling af mekanisk energi er af betydning.

Selvom hovedproblemet er løsning af randværdiproblemet ligger de interessante karakteristika ligger i det lydfelt, som dannes af en påtrykt elektrisk spænding og vice versa. Der behandles udelukkende funktioner med harmonisk tidsvariation, som repræsenteres ved den implicitte tidsfaktor, $e^{-i\omega t}$. De behandlede piezoelektriske materialer tilhører gruppen af polariserede ferroelektriske keramikker, som alle er ortotrope.

Problemet med vibrationer i tykkelsesretningen af en uendelig piezoelektrisk plade spiller en væsentlig rolle i design af piezoelektriske ultralydtransducere. Der præsenteres en løsning på sluttet form, som bliver anvendt til at bestemme komponentværdier i et simpelt elektrisk ækvivalent diagram.

På grund af de piezoelektriske ligningers kompleksitet er løsninger på sluttet form undtagelsen snarere end de er reglen. Det er derfor nødvendigt at anvende tilnærmede metoder. Af disse tages følgende i betragtning: Ækvivalent diagrammer, Rayleigh-Ritz metoden, Mindlin plade teori og finite element metoden.

Finite element metoden er blevet udnyttet til analyse af aksesymmetriske transducere. Der præsenteres et eksplicit, piezoelektrisk ring element med trekantet tværsnit og lineære variationer i flytningerne og i det elektriske potential. Indflydelsen fra et vædskefyldt halv-rum præsenteres i form af en kompleks stivhedsmatrix.

En transducer kan ligeledes være forsynet med en såkaldt backing. Denne antages at være cylindrisk og modelleres som en række iden-

tiske lag. Der anvendes herefter en særlig procedure, som hurtigt og billigt kan kombinere lagene. Der gives også anvisning på, hvorledes en lignende metode kan anvendes på uendelige bølgeledere.

Resultaterne, som er opnået med finite element metoden, er blevet sammenlignet med målinger og eksakte løsninger med godt resultat.

Det konkluderes, at finite element metoden kan være et værdifuldt værktøj til at analysere og designe ultralydtransducere.

LIST OF SYMBOLS

a	: Radius of circular disk.
A	: Area.
c	: Velocity.
c_p	: velocity of pressure waves.
c_g, c_ϕ	: Group velocity, phase velocity.
C	: Capacitance.
C_{pq}, C_{ijkl}	: Elastic constants.
C_{mn}, $C_{\alpha\beta}^{ij}$	: Damping matrix.
D_i, D_α	: Electric displacement.
D_{mn}, $D_{\alpha\beta}^{mn}$	: Dynamic stiffness matrix.
e_{ijk}, $e_{\alpha\beta}$	: Piezoelectric constants.
E_i, E_α	: Electric field vector.
f_i^S, f_i^V	: Surface, volume force.
F_j^m	: Nodul force.
G	: Functional.
h	: (half) thickness of plate.
H	: Electrical enthalpy.
$H_\nu()$	: Hankel function of order ν.
$H_\nu()$	: Struve function of order ν.
i	: The imaginary unit.
$I_\nu()$	: Modified Bessel function of order ν.
$J_\nu()$	: Bessel function of order ν.
k	: Wave number.
K	: Spring constant.
K_ν	: Modified Hankel function of order ν.

K_{mn}, $K_{\alpha\beta}^{mn}$: Stiffness matrix.

ℓ_α^i : Side vector in triangular element.

L : Lagrangian.

L : Inductance.

M : Mass.

M_{mn}, $M_{\alpha\beta}^{mn}$: Mass matrix.

n_i : Normal vector.

n_α^i : Side normal in triangular element.

1:N : Voltage ratio for transformer.

N_t : Thickness frequency constant.

$N_k^N()$, $N_4^n()$: Shape function.

p : Pressure.

p^o : Pressure on surface of half-space

p_n : Expression coefficient for p^o.

$P_n()$: Legender polynomial of order n.

q^s, q^v : Surface or volume electric charge.

Q^m : Nodal electric charge.

r : Distance from a (source) point.

R : Resistance.

S_p, S_{ij} : Strain vector or tensor.

T_p, T_{ij} : Stress vector or tensor.

u_i, u_α : Displacement.

u_i^n : Nodal displacement.

U : The internal energy.

v : Velocity of a body.

v^o : Normal velocity on surface of half-space.

v_n : Expansion coefficient of v^o.

V : Volume.

W : Work.

X_i, X_α : Space coordinate.

x_α^n : Space coordinate to a node.

x_α^e : Mean space coordinate of the corners in a triangle.

Z : Acoustic impedance

Z_{mn} : Generalized impedance matrix

$Z_\pm$: (half) sum and difference of the acoustic impedances on the two faces of a plate.

$\alpha(\omega)$: Attenuation.

β : Propagation constant.

γ : Frequency exponent.

$\delta \cdot$: Variation of $\cdot$.

$\delta_{ij}, \delta_{ijk}$: Kronecker delta.

$\varepsilon_{ij}, \varepsilon_{\alpha\beta}$: Dielectric constants.

θ : Angle.

θ : Temperature (sec. 2).

λ_i : Area coordinate.

ν, ν_p : Poissons ratio, planar.

ρ : Mass density.

σ : Entropy (sec. 2).

$\tau_\pm$: (half) sum and difference of the normal stress on the two faces of a plate.

ϕ : Electric potential.

ϕ : Angle.

ϕ^n : Nodal electric potential.

Φ_- : (half) potential difference between the two faces of a plate.

ψ : Velocity potential (in a fluid).

ω : Angular frequency.

APPENDIX A: Material data

The material data used as input to the finite element program are listed below for the materials which are mentioned in this thesis and a few other which have been used for tests.

Fluids:	Water	Air
ρ [kg/m^3]	1000	1.20
C_{11} [G Pa]	2.25	$0.135 \cdot 10^{-3}$

Backing material:	Epoxy and filler
ρ [kg/m^3]	4870
C_{11} [G Pa]	17.14-i 3.80
C_{55} [G Pa]	3.89-i 1.00

Piezoelectrics:	PZT-5A	PZT-5H
ρ [kg/m^3]	7750	7500
C_{11} [G Pa]	121.0	126.0
C_{12} [G Pa]	75.4	79.5
C_{13} [G Pa]	75.2	84.1
C_{33} [G Pa]	111.0	117.0
C_{55} [G Pa]	21.1	23.0
ε_{11} [nF/m]	8.1	15.0
ε_{33} [nF/m]	7.3	13.0
e_{13} [C/m^2]	-5.4	-6.5
e_{33} [C/m^2]	15.8	23.3
e_{51} [C/m^2]	12.3	17.0
N_t [Hz·m]	1890	2000

APPENDIX B: Contour Integration

The generalized impedance matrix Z_{mn} is given by the infinite integral (5.16)

$$Z_{mn} = \int_0^\infty \frac{J_{2m+1}(bs)J_{2n+1}(bs)}{s\beta(s)}\,ds \tag{B1}$$

where b = ka and

$$\beta(s) = \begin{cases} \sqrt{s^2-1} & \text{for } s > 1 \\ i\sqrt{1-s^2} & \text{for } s < 1 \end{cases} \tag{B2}$$

This integral is not well-suited to numerical calculation due to the oscillatory behaviour of the integrand. By contour integration similar to that of [64, Appendix A] , the integrand can be expressed in a more suitable form. In the complex plane $\beta(S)$ must have a branch cut which is taken to be the part of the real axis for thich $-1 < \mathrm{Re}\{s\} < 1$. $\beta(s)$ is discontinuous across the branch cut and the two sides are connected by $\beta(s+i\varepsilon) \to -\beta(s-i\varepsilon)$ for $\varepsilon \to 0$ when s is real and $-1 < s < 1$.

As $Z_{mn} = Z_{nm}$ it is no restriction to assume $m > n$ which will be done from now on. $J_{2n+1}()$ is then replaced by

$$J_{2n+1}(bs) = 1/2(H^{(1)}_{2n+1}(bs) + H^{(2)}_{2n+1}(bs)) \tag{B3}$$

and the integral is written as two integrals, one with $H^{(1)}()$ and one with $H^{(2)}()$. The asymptotic behaviour of the Hankel functions for large values of Z is given by

$$H^{(1,2)}_\nu \sim \sqrt{\frac{2}{\pi z}}\, e^{\pm i(z-\nu\pi/2-\pi/4)} \tag{B4}$$

the integrand with $H^{(1)}_{2n+1}(bs)$ therefore behaves asymptotically as $|s|^{-3}$ in the half-plane $\mathrm{Im}\{s\} > 0$ while that with $H^{(2)}_{2n+1}(bs)$ be-

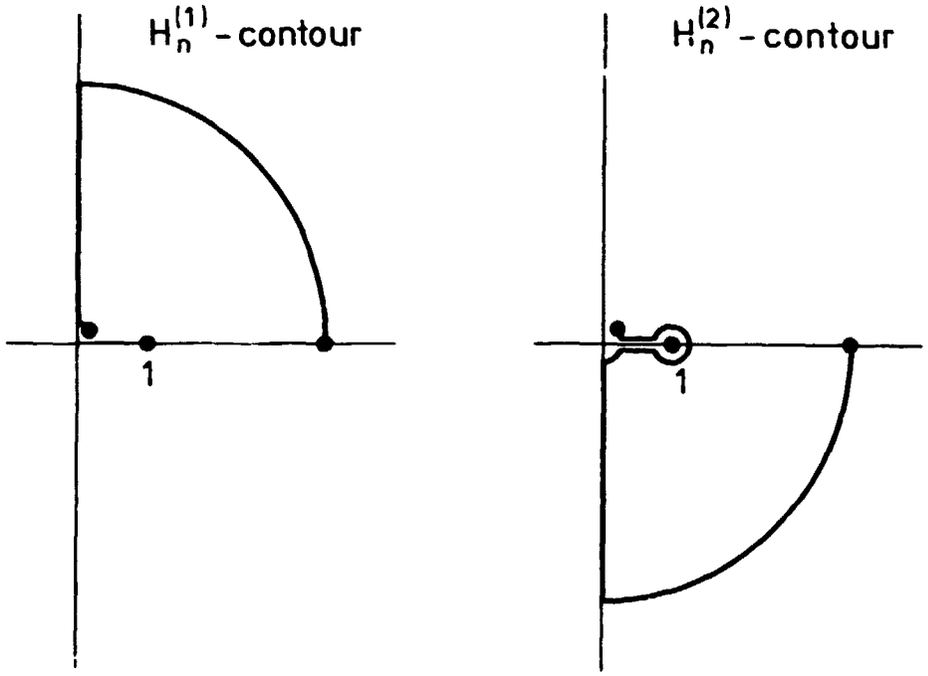

Fig. B.1. Integration contours in the complex s-plane.

haves like $|s|^{-3}$ in the half-plane Im $\{s\} < 0$. For this reason the two integrals are integrated along different paths, as shown on Fig. B.1.

The large circles gives zero contribution to the integral as the length is proportional only to $|s|^2$. The pole at $s = 0$ in (B1) is removeable, but after the reorganization the Hankel functions introduces a logarithmic singularity, and the integral must be found by a limit process

$$Z_{mn} = \lim_{\varepsilon \to 0} \left\{ \int_{\varepsilon}^{1-\varepsilon} \frac{J_{2m+1}(bs) H_{2n+1}^{(2)}(bs)}{s\, \beta(s)}\, ds \right.$$

$$+ 1/2 \int_{-i\varepsilon}^{-i\infty} \frac{J_{2m+1}(bs) H_{2n+1}^{(2)}(bs)}{s\, \beta(s)}\, ds$$

$$\left. + 1/2 \int_{i\varepsilon}^{i\infty} \frac{J_{2m+1}(bs) H_{2n+1}^{(1)}(bs)}{s\, \beta(s)}\, ds \right\} \qquad \text{(B5)}$$

The substitution s = -is on the negative imaginary axis and s = is on the positive part then gives

$$Z_{mn} = \lim_{\varepsilon \to 0} \left\{ -i \int_{\varepsilon}^{i-\varepsilon} \frac{J_{2m+1}(bs) H^{(2)}_{2n+1}(bs))}{s\sqrt{1-s^2}}\, ds \right.$$

$$\left. - (-1)^{m-n} \frac{2}{\pi} \int_{\varepsilon}^{\infty} \frac{I_{2m+1}(bs) K_{2n+1}(bs)}{s\sqrt{1+s^2}}\, ds \right\} \qquad \text{(B6)}$$

where $I_{2m+1}()$ and $K_{2n+1}()$ are the modified Bessel functions.

Finally, the trigonometric substitution $s = \sin\theta$ in the finite integral and $s = \tan\theta$ in the infinite integral gives

$$Z_{mn} = - \int_{0}^{\frac{\pi}{2}} \left\{ i\, J_{2m+1}(b\sin\theta) H^{(2)}_{2n+1}(b\sin\theta) \right.$$

$$\left. + (-1)^{m-n} \frac{2}{\pi} I_{2m+1}(b\tan\theta) K_{2n+1}(b\tan\theta) \right\} \frac{d\theta}{\sin\theta} \qquad \text{(B7)}$$

Risø National Laboratory **Risø – R – 536**

Title and author(s)

Calculations for Piezoelectric Ultrasonic Transducers

Henrik Jensen

Date May 1986

Department or group

Metallurgy Dept.

Groups own registration number(s)

Project/contract no.

Pages 97 Tables 5 Illustrations 24 References 64

ISBN 87-550-1198-5

Abstract (Max. 2000 char.)

Analysis of piezoelectric ultrasonic transducers implies a solution of a boundary value problem, for a body which consists of different materials, including a piezoelectric part. The problem is dynamic at frequencies, where a typical wavelength is somewhat less than the size of the body. Radiation losses as well as internal losses may be important. Due to the complexity of the problem, a closed form solution is the exception rather than the rule. For this reason, it is necessary to use approximate methods for the analysis.

Equivalent circuits. the Rayleigh-Ritz method, Mindlin plate theory and in particular the finite element method are considered. The finite element method is utilized for analysis of axisymmetric transducers. An explicit, fully piezoelectric, triangular ring element, with linear variations in displacement and electric potential is given. The influence of a fluid hal-space is also given, in the form of a complex stiffness matrix.

A special stacking procedure, for analysis of the backing has been developed. This procedure gives a saving, which is similar to that of the fast fourier transform algorithm, and is also wellsuited for analysis of finite and infinite waveguides.

Results obtained by the finite element method are shown and compared with measurements and exact solutions. Good agreement is obtained.

It is concluded that the finite element method can be a valueable tool in analysis and design of ultrasonic transducers.

Descriptors – INIS:

AXIAL SYMMETRY; EQUIVALENT CIRCUITS; FINITE ELEMENT METHOD; PIEZOELECTRICITY; RESONATORS; TRANSDUCERS; ULTRASONIC WAVES; WAVEGUIDES

Available on request from Risø Library, Risø National Laboratory, (Risø Bibliotek, Forsøgsanlæg Risø), P.O. Box 49, DK-4000 Roskilde, Denmark.
Telephone (02) 37 12 12, ext. 2262. Telex: 43116, Telefax: (02) 36 06 09

Sales distributors:
G.E.C. Gad Strøget
Vimmelskaftet 32
DK-1161 Copenhagen K, Denmark

Available on exchange from:
Risø Library, Risø National Laboratory,
P.O.Box 49, DK-4000 Roskilde, Denmark

ISBN 87-550-1198-5
ISSN 0106-2840